

Sea-surface temperature pattern effects have slowed global warming and biased warming-based constraints on climate sensitivity

Article

Accepted Version

Armour, K. C., Proistosescu, C., Dong, Y., Hahn, L. C., Blanchard-Wrigglesworth, E., Pauling, A. G., Wills, R. C. J., Andrews, T., Stuecker, M. F., Po-Chedley, S., Mitevski, I., Forster, P. M. and Gregory, J. M. ORCID: <https://orcid.org/0000-0003-1296-8644> (2024) Sea-surface temperature pattern effects have slowed global warming and biased warming-based constraints on climate sensitivity. *Proceedings of the National Academy of Sciences of the United States of America*, 121 (12). e2312093121. ISSN 0027-8424 doi: 10.1073/pnas.2312093121 Available at <https://centaur.reading.ac.uk/115193/>

It is advisable to refer to the publisher's version if you intend to cite from the work. See [Guidance on citing](#).

To link to this article DOI: <http://dx.doi.org/10.1073/pnas.2312093121>

Publisher: National Academy of Sciences

All outputs in CentAUR are protected by Intellectual Property Rights law, including copyright law. Copyright and IPR is retained by the creators or other copyright holders. Terms and conditions for use of this material are defined in the [End User Agreement](#).

www.reading.ac.uk/centaur

CentAUR

Central Archive at the University of Reading

Reading's research outputs online

Sea-surface temperature pattern effects have slowed global warming and biased warming-based constraints on climate sensitivity

Kyle C. Armour^{a,b,1,2}, Cristian Proistosescu^{c,1}, Yue Dong^d, Lily C. Hahn^e, Edward Blanchard-Wrigglesworth^a, Andrew G. Pauling^f, Robert C. Jnglin Wills^{a,g}, Timothy Andrews^h, Malte F. Stueckerⁱ, Stephen Po-Chedley^j, Ivan Mitevski^k, Piers M. Forster^l, and Jonathan M. Gregory^{h,m}

^aDepartment of Atmospheric Sciences, University of Washington, Seattle, WA, USA; ^bSchool of Oceanography, University of Washington, Seattle, WA, USA; ^cDepartment of Atmospheric Sciences and Department of Geology, University of Illinois Urbana-Champaign, Champaign, IL, USA; ^dCIRES, University of Colorado, Boulder, CO, USA; ^eScripps Institution of Oceanography, La Jolla, CA, USA; ^fDepartment of Physics, University of Otago, Dunedin, NZ; ^gInstitute for Atmospheric and Climate Science, ETH Zurich, Zurich, CH; ^hMet Office Hadley Centre, Exeter, UK; ⁱDepartment of Oceanography and International Pacific Research Center, School of Ocean and Earth Science and Technology, University of Hawai'i at Mānoa, HI, USA; ^jProgram for Climate Model Diagnosis and Intercomparison, Lawrence Livermore National Laboratory, Livermore, CA, USA; ^kDepartment of Applied Physics and Applied Mathematics, Columbia University, New York, NY, USA; ^lPriestley International Centre for Climate, University of Leeds, Leeds, UK; ^mNational Centre for Atmospheric Science, University of Reading, Reading, UK

This manuscript was compiled on November 10, 2023

1 The observed rate of global warming since the 1970s has been pro-
2 posed as a strong constraint on equilibrium climate sensitivity (ECS)
3 and transient climate response (TCR) – key metrics of the global
4 climate response to greenhouse-gas forcing. Using CMIP5/6 mod-
5 els, we show that the inter-model relationship between warming and
6 these climate sensitivity metrics (the basis for the constraint) arises
7 from a similarity in transient and equilibrium warming patterns within
8 the models, producing an effective climate sensitivity (EffCS) gov-
9 erning recent warming that is comparable to the value of ECS gov-
10 erning long-term warming under CO₂ forcing. However, CMIP5/6
11 historical simulations do not reproduce observed warming patterns.
12 When driven by observed patterns, even high ECS models produce
13 low EffCS values consistent with the observed global warming rate.
14 The inability of CMIP5/6 models to reproduce observed warming pat-
15 terns thus results in a bias in the modeled relationship between
16 recent global warming and climate sensitivity. Correcting for this
17 bias means that observed warming is consistent with wide ranges
18 of ECS and TCR extending to higher values than previously recog-
19 nized. These findings are corroborated by energy balance model sim-
20 ulations and coupled model (CESM1-CAM5) simulations that better
21 replicate observed patterns via tropospheric wind nudging or Antarc-
22 tic meltwater fluxes. Because CMIP5/6 models fail to simulate ob-
23 served warming patterns, proposed warming-based constraints on
24 ECS, TCR, and projected global warming are biased low. The results
25 reinforce recent findings that the unique pattern of observed warm-
26 ing has slowed global-mean warming over recent decades, and that
27 how the pattern will evolve in the future represents a major source of
28 uncertainty in climate projections.

climate sensitivity | global warming | climate dynamics

1 **E**quilibrium climate sensitivity (ECS) and transient cli-
2 mate response (TCR) are key metrics of the global-mean
3 surface temperature response to increasing greenhouse-gas
4 concentrations. They represent the warming under a doubling
5 of atmospheric carbon dioxide (CO₂) at equilibrium and at the
6 time of CO₂ doubling, respectively. Model values of ECS and
7 TCR are strongly correlated with projections of 21st century
8 warming (1, 2). The recent IPCC Sixth Assessment Report
9 (AR6) assessed the ranges of ECS and TCR to be substantially
10 more narrow than in previous Reports (2) following advances
11 in scientific understanding of several independent lines of ob-
12 servational evidence (e.g., 3). Narrower ranges of ECS and

TCR in turn translate to better-constrained projections of
21st century warming compared to projections based on global
climate models (GCMs), which span wider ECS and TCR
ranges (4).

One major update in IPCC AR6 was a reinterpretation
of historical energy budget constraints on climate sensitivity
based on observed warming since the 1800s. While the
historical energy budget was once thought to place strong
constraints on ECS (5–7), in IPCC AR6 it was assessed to pro-
vide relatively weak constraints, particularly at the high end
of the climate sensitivity range. This assessment was based
on (i) stubbornly-large uncertainty in the radiative forcing
that drove historical warming, owing primarily to uncertainty
in aerosol forcing, and (ii) work since AR5 showing that dif-
ferences between historical and future (centennial timescale)
sea-surface temperature (SST) trend patterns result in esti-
13
14
15
16
17
18
19
20
21
22
23
24
25
26
27
28

Significance Statement

Global climate models show a tight relationship between post-1970s global warming and climate sensitivity. The latest IPCC Assessment Report (AR6) used observations of the warming rate as a key piece of evidence constraining Earth's climate sensitivity and warming projections. However, climate models do not reproduce the observed spatial pattern of warming, introducing a bias in the modeled warming-sensitivity relationship that results in overly-confident constraints on climate sensitivity. The findings suggest that observed warming over recent decades provides very little information about climate sensitivity, and that constraints on high climate sensitivity values must come from other lines of observational evidence. Additionally, projections of global warming need to account for how the spatial pattern of warming will evolve in the future. Since climate models fail to reproduce recent patterns, this introduces a major uncertainty in climate projections.

K.C.A. and C.P. designed and performed the research; Y.D., E.B.W., A.G.P., M.F.S., and J.M. contributed numerical simulations; K.C.A., C.P., L.C.H., and R.J.W. analyzed data; and K.C.A. wrote the paper with contributions from all authors.

The authors declare no competing interests.

¹K.C.A. contributed equally to this work with C.P.

²To whom correspondence should be addressed. E-mail: karmour@uw.edu

29 mates of ECS that are biased low (2, 3, 8–19). This SST
30 *pattern effect* occurs because the feedbacks governing Earth's
31 global radiative response per degree of global warming depend
32 on the spatial pattern of that warming. In particular, warming
33 since the 1800s has been relatively slow within key regions
34 of positive (destabilizing) radiative feedbacks including the
35 eastern tropical Pacific Ocean and Southern Ocean; in the long
36 term, however, these regions are expected to warm more than
37 the global mean, leading to a less-negative global feedback and
38 thus an increase in the climate's sensitivity to greenhouse-gas
39 forcing (8, 9, 19–27). Thus, the value of the *effective* climate
40 sensitivity (EffCS) governing historical warming is thought to
41 be lower than the value of ECS governing equilibrium warming
42 under CO₂ forcing (2, 3).

43 Another major advance in recent years has been the de-
44 velopment of novel observational constraints (often referred
45 to as “emergent constraints”), wherein coupled GCMs are
46 used to find a correlation between an observable quantity and
47 something we wish to predict, and then the model-based re-
48 lationship is combined with observations of that quantity to
49 derive constrained predictions (28–31). Strong constraints on
50 ECS and TCR have been derived using the post-1970s rate of
51 global-mean warming (18, 32–34): because GCMs with higher
52 ECS and TCR values tend to overestimate the observed rate
53 of warming, the implication is that high values of climate sensi-
54 tivity are less likely. This constraint was proposed to avoid the
55 issues plaguing energy budget constraints based on warming
56 since the 1800s (32): because global aerosol radiative forcing
57 changes have been relatively small since the 1970s, the use
58 of this period substantially reduces the impact of uncertainty
59 in radiative forcing; and SST pattern effects are implicitly
60 accounted for in the use of GCMs to derive the correlation
61 between recent warming and ECS (or TCR).

62 As summarized in Forster et al. (2), studies using post-
63 1970s global warming as an observational constraint produce
64 narrow bounds on ECS (with best estimates of 2.6–2.8°C and
65 5–95% ranges within 1.5–4.1°C) and TCR (with best estimates
66 of 1.6–1.7°C and 5–95% ranges within 1.0–2.3°C). Collectively,
67 these studies provided the strongest constraints on ECS and
68 TCR of any of the main lines of evidence assessed in IPCC
69 AR6, and were a primary justification for assessing the upper
70 bounds on the ECS *likely* (2.5–4°C) and *very likely* (2–5°C)
71 ranges to be lower than in previous Reports. These narrower
72 ranges also suggest that GCMs with ECS values higher than
73 about 5°C, of which there are many (35) in the Coupled Model
74 Intercomparison Project phase 6 (CMIP6, ref. 36), may be
75 less valid for projecting future warming (e.g., 2, 37).

76 For such a constraint to be robust, it must exhibit two key
77 properties. First, because many spurious correlations between
78 observable and predicted quantities of interest can be found by
79 chance within GCMs (38), any correlation that is used as the
80 basis for the constraint must rest on sound physical principles
81 (28, 29, 31, 39). Second, the GCMs used as the basis for the
82 constraint must not share a common bias, relative to nature,
83 in their representation of this correlation (e.g., 28, 40).

84 For constraints on ECS and TCR based on observed post-
85 1970s global warming, there is a strong physical basis for the
86 modeled correlation: higher ECS and TCR correspond to a
87 less-efficient radiative response per degree of global warming
88 which, all else being equal, should lead to a faster rate of global
89 warming under greenhouse-gas forcing. And the constraints

90 have been shown to produce similar results whether using
91 CMIP5 or CMIP6 models (18, 32–34), providing confidence
92 in their robustness.

93 However, recent work has found that historical simulations
94 of CMIP5/6 models generally fail to simulate the observed
95 spatial pattern of post-1970s SST trends (16, 17, 41, 42). In
96 particular, the models produce relatively weak spatial gradients
97 in SST trends, with somewhat enhanced warming in the
98 eastern tropical Pacific Ocean and at high latitudes, while
99 observations show strong spatial gradients in SST trends, with
100 cooling in the eastern Pacific and Southern Oceans.

101 These model-versus-observed discrepancies in SST trend
102 patterns influence the radiative feedbacks that govern climate
103 sensitivity: when atmosphere GCMs are forced with the ob-
104 served post-1970s SST trends, they generally produce global
105 radiative feedbacks that are substantially more negative (lower
106 EffCS) than feedbacks produced over this period by historical
107 simulations of the same coupled GCMs (16, 17). This suggests
108 that there *is* in fact a common bias across CMIP5/6 GCMs
109 that could affect the modeled relationship between post-1970s
110 warming and climate sensitivity metrics. It is possible, for
111 instance, that GCMs overestimate recent warming in part due
112 to their biases in simulated warming patterns, with relatively
113 too much warming in key positive feedback regions, rather
114 than simply having too-high values of ECS or TCR (as is
115 assumed by the observational constraint). IPCC AR6 noted
116 this possibility, finding it *more likely than not* that constraints
117 on ECS and TCR based on observed post-1970s global warm-
118 ing are biased low (2); but without studies quantifying the
119 magnitude of this bias, no corrections could be made.

120 Here we evaluate the potential for SST pattern effects to
121 bias observational constraints on ECS and TCR via their influ-
122 ence on the CMIP5/6-based relationship between post-1970s
123 global warming and these climate sensitivity metrics. We
124 first reproduce constraints on ECS and TCR based on recent
125 warming and find similar results to the published literature.
126 We then analyze a subset of CMIP5/6 models that provide the
127 output necessary to accurately calculate radiative feedbacks
128 (and corresponding EffCS) over the historical period. We find
129 that CMIP5/6 models warm too much over recent decades in
130 large part due to their failure to replicate the observed post-
131 1970s SST trend patterns, and thus even high values of climate
132 sensitivity are consistent with the observed global warming
133 rate. We conclude that the proposed constraints on ECS and
134 TCR based on recent global warming are biased low. We
135 evaluate the robustness of our findings using energy-balance
136 model simulations and coupled-model (CESM1-CAM5) sim-
137 ulations that better replicate observed patterns via tropospheric
138 wind nudging or Antarctic meltwater fluxes. Finally, we dis-
139 cuss implications of these results for recent climate sensitivity
140 assessments and for 21st century warming.

141 The relationship between post-1970s warming and cli- 142 mate sensitivity

143 While several different time periods have been used to place
144 observational constraints on climate sensitivity from recent
145 global warming (32, 33), here we focus on 1981–2014 following
146 Tokarska et al. (34). We show relationships between the rate
147 of global-mean surface warming over this period and ECS (Fig.
148 1a) for all GCMs that provide the necessary output on the
149 CMIP5/6 archives (21 CMIP5 models and 38 CMIP6 models;

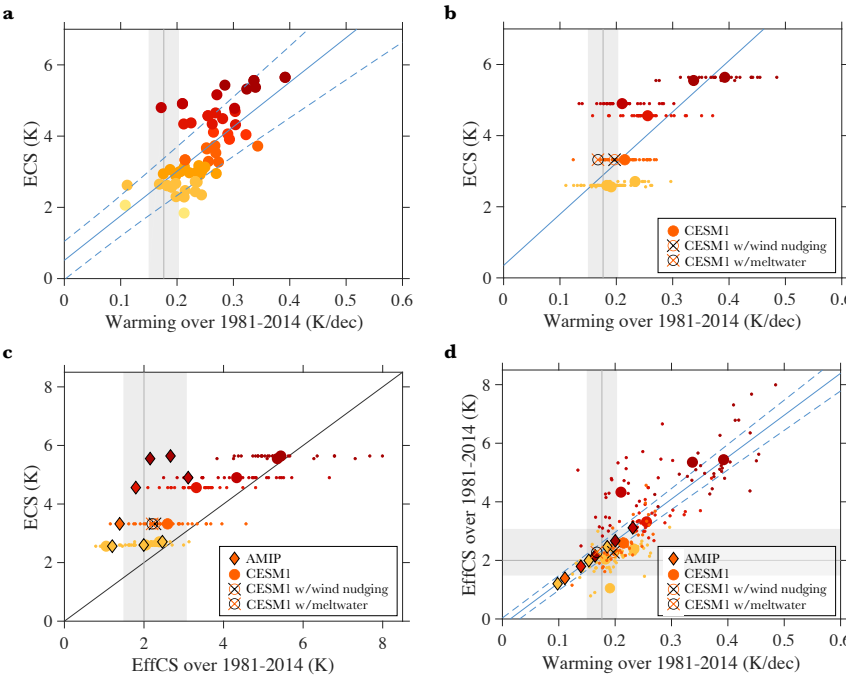


Fig. 1. Relationships between equilibrium climate sensitivity (ECS), effective climate sensitivity (EffCS), and the 1981–2014 warming rate in CMIP5/6 models. **a**, CMIP5/6 ECS versus warming rate using averages of all available ensemble members for each model (correlation $r = 0.68$); colors correspond to values of ECS. **b**, Eight-model subset ECS versus warming rate with ensemble means shown as larger circles and ensemble members shown as smaller dots. **c**, Eight-model subset ECS versus EffCS over 1981–2014 with ensemble means shown as larger circles and ensemble members shown as smaller dots; diamonds show EffCS values from AGCM simulations forced by observed SST and SIC trend patterns. **d**, Eight-model subset EffCS over 1981–2014 versus warming rate with ensemble means shown as larger circles and ensemble members shown as smaller dots; diamonds show warming rates estimated based on EffCS values from AGCM simulations using the regression between EffCS and warming rate calculated from the eight-model subset (blue line). In **b–d**, open circles show CESM1-CAM5 simulations with wind nudging or meltwater fluxes as described in the text. Blue lines show fits calculated using ordinary least squares regression, with dashed blue lines showing 5–95% ranges of fit parameters (Methods). Gray shading shows observational estimates (5–95% range) of observed warming rate (HadCRUT5, ref. 45) and EffCS (19). See Supplementary Information for a list of models used.

see Supplementary Information for a list). While we focus on ECS in the main text, the full analysis using TCR produces similar results (Supplementary Information). We calculate warming rates by averaging over all available ensemble members of each model's *historical* simulation (extended using RCP4.5 over years 2006–2014 for CMIP5 models), where each ensemble member is forced by identical historical greenhouse-gas, aerosol, volcanic, and solar forcings, and differ only in their phasing of internal variability. CMIP5/6 model values of ECS have been estimated using the standard approach of extrapolating to equilibrium the regression between global top-of-atmosphere energy imbalance and global temperature change over 150 years of abrupt CO₂ quadrupling simulations, scaled by a factor of a half to account for CO₂ doubling (35, 43, 44).

We find a strong correlation between the 1981–2014 global warming rate and ECS (Fig. 1a) or TCR (Fig. S1a). Using this regression (Methods), the observed warming rate of 0.18°C dec⁻¹ (0.15–0.21°C dec⁻¹, 5–95% range) calculated from HadCRUT5 (45) gives ECS = 2.7°C (1.5–3.9°C) and TCR = 1.6°C (1.1–2.1°C), in good agreement with previous studies (18, 32–34).

To better understand the modeled relationship between global warming and climate sensitivity, we consider a subset of eight CMIP5/6 models representing all those that provide at least three *historical* ensemble members and the output necessary to accurately calculate radiative feedbacks over the historical period: CanESM5, CNRM-CM6-1, GISS-E2-1-G, HadGEM3-GC31-LL, IPSL-CM6A-LR, MIROC6, NorESM2-LM, and CESM1-CAM5. The relationships between 1981–2014 global warming rate and ECS are similar for this eight-model subset (Fig. 1b) to those found in the full CMIP5/6 ensemble (Fig. 1a). For each model, there is substantial spread in warming rates across ensemble members due to internal climate variability (Fig. 1b), raising two key questions: (i) What factors control the variability in warming rates across model ensemble

members? And, (ii) do CMIP5/6 models accurately represent how those factors were expressed in observations over the period 1981–2014?

Each of the eight models in our subset has a corresponding CMIP6 *piClim-histall* simulation wherein the same atmosphere GCM (AGCM) was run with fixed pre-industrial SSTs and sea-ice concentrations (SICs) while all radiative forcing agents were varied as in the corresponding CMIP6 *historical* simulations. The *piClim-histall* simulations were performed as part of the Radiative Forcing Model Intercomparison Project (RFMIP, ref. 46) for CMIP6, while we perform our own *piClim-histall*-style simulation for CESM1-CAM5 following the same protocol. From these simulations, the historical effective radiative forcing (ERF) can be diagnosed from top-of-atmosphere radiation anomalies relative to pre-industrial conditions (17, 47), with a small correction for land warming (2, 48) (Methods). Using the standard model of global energy balance,

$$N = \lambda T + \text{ERF}, \quad [1]$$

where N is the global top-of-atmosphere radiation anomaly and T is the global near-surface air temperature anomaly (both relative to pre-industrial), we diagnose the global *effective* radiative feedback λ (< 0 for a stable climate) from linear regression of $N - \text{ERF}$ against T over the period 1981–2014 for each ensemble member (Methods). From this, we calculate EffCS for the period 1981–2014 as,

$$\text{EffCS} = -\frac{\text{ERF}_{2\times}}{\lambda}, \quad [2]$$

where $\text{ERF}_{2\times}$ is the effective radiative forcing from CO₂ doubling (35, 44) (Methods). EffCS is largely set by the value of λ both because it is in the denominator in equation (2) and because λ varies fractionally more than does $\text{ERF}_{2\times}$ across models (35). EffCS can be interpreted as the equilibrium warming that would occur in response to CO₂ doubling if the value of λ calculated over the period 1981–2014 applied to that equilibrium state.

220 We find that there is a large spread in EffCS for the period
 221 1981-2014 across ensemble members of each GCM (small dots
 222 in Fig. 1c). Moreover, differences in EffCS explain a large
 223 fraction of the variance ($r^2 = 0.61$) in the 1981-2014 warming
 224 rate across all ensemble members of our eight-model subset;
 225 those with EffCS values near 2°C tend to produce warming
 226 rates in line with observations, while those with higher values
 227 of EffCS warm too much (Fig. 1d).

228 The high correlation between EffCS and the global warming
 229 rate can be understood by making the approximation $N = \kappa T$
 230 in equation (1), where κ is the ocean heat uptake efficiency
 231 representing all processes setting the amount of global ocean
 232 heat uptake per degree of global warming (e.g., 49–51); a
 233 larger value of κ corresponds to a more efficient uptake of heat
 234 by the deep ocean and thus less surface warming. Then, the
 235 rate of warming can be approximated as (e.g., 52),

$$\frac{dT}{dt} = \frac{d(\text{ERF})/dt}{\kappa - \lambda}. \quad [3]$$

236 Calculating κ from regression of N against T over 1981-2014,
 237 and given $d(\text{ERF})/dt$ and λ as calculated above, equation
 238 (3) explains 83% of the variance in the 1981-2014 warming
 239 rate across all ensemble members of our CMIP5/6 model
 240 subset. Most of the explanatory power comes from variations
 241 in λ : holding κ and $d(\text{ERF})/dt$ fixed at ensemble-mean values,
 242 equation (3) still explains 58% of the variance across ensemble
 243 members. That is, variations in λ (and thus EffCS) largely
 244 govern the global warming rate, with variations in κ playing a
 245 secondary role. There is little correlation between λ and κ on
 246 the timescales considered here (Methods), so we treat them
 247 as independent for our purposes.

248 Using the regression between EffCS and the 1981-2014
 249 warming rate derived from the eight-model subset (Fig. 1d),
 250 the observed warming rate of 0.18 (0.15 – 0.21) $^{\circ}\text{C dec}^{-1}$ im-
 251 plies EffCS = 2.3 (1.9 – 2.7) $^{\circ}\text{C}$. While on the low end of the
 252 CMIP5/6 models (Fig. 1d), this implied value of EffCS is in
 253 good agreement with a recent observational estimate (19) of
 254 EffCS = 2.0 (1.5 – 3.1) $^{\circ}\text{C}$ based on global energy imbalance
 255 calculated from a merged satellite dataset (53) in combination
 256 with ERF estimates from IPCC AR6 (2) and HadCRUT5 tem-
 257 perature observations over 1985-2014. The CMIP5/6-based
 258 relationship between EffCS and warming rate thus compares
 259 well with observations.

260 Importantly, EffCS may be different from ECS, which is
 261 given by

$$\text{ECS} = -\frac{\text{ERF}_{2\times}}{\lambda_{2\times}}, \quad [4]$$

262 owing to the fact that the radiative feedback λ governing
 263 recent warming may be different from the radiative feedback
 264 $\lambda_{2\times}$ governing the equilibrium response to CO₂ doubling if
 265 warming patterns differ between the two timescales. Given
 266 that ECS is a measure of the *equilibrium* climate response to
 267 CO₂ forcing, it is worth considering why it is highly correlated
 268 with the rate of *transient* warming over 1981-2014 in CMIP5/6
 269 models (Figs. 1a,b). The reason appears to be that values of
 270 ECS and ensemble-mean EffCS are nearly identical for each
 271 of the CMIP5/6 models (Fig. 1c); EffCS is similar to but
 272 slightly smaller than ECS for most of the GCMs, with a high
 273 correlation between them ($r^2 = 0.70$).

274 These findings are consistent with the fact that the spatial
 275 patterns of historical warming (setting EffCS over 1981-
 276 2014) and equilibrium warming under abrupt CO₂ forcing

277 (setting ECS) are similar in CMIP5/6 models (Figs. 2a,b) (17);
 278 both are characterized by relatively weak spatial gradients
 279 in SST trends. That is, the relationship between ECS and
 280 the 1981-2014 warming rate, which forms the basis for the
 281 observational constraint, reflects similar patterns of transient
 282 and equilibrium warming within the coupled CMIP5/6 models,
 283 corresponding to a relatively small pattern effect (i.e., values
 284 of EffCS governing recent warming are comparable to values
 285 of ECS governing long-term warming).

286 As noted in the introduction, the observed SST trend pat-
 287 tern over 1981-2014 (Fig. 2c) is distinct from patterns sim-
 288 ulated by the coupled CMIP5/6 models (17, 41, 42). With
 289 strong warming in the western tropical Pacific Ocean (a region
 290 of negative feedbacks) and cooling in the eastern Pacific and
 291 Southern Oceans (regions of positive feedbacks), the observed
 292 pattern should favor a low value of EffCS (8, 9, 14, 16, 17, 19–
 293 27) and thus a reduced global warming rate (equation (3)).
 294 This observed pattern of warming is also distinct from the
 295 long-term warming pattern we expect under CO₂ forcing (2),
 296 suggesting that the relationship between EffCS (governing
 297 recent warming) and ECS (governing long-term warming) in
 298 nature may be different from that simulated by CMIP5/6
 299 models. In the next section, we consider how model SST trend
 300 biases may, in turn, bias the warming-sensitivity relationship
 301 which forms the basis for the observational constraint.

Impact of model SST trend biases on the warming-sensitivity relationship

302 To quantify the impact of the SST trend pattern on global
 303 warming rate, we make use of *amip* simulations wherein the
 304 same subset of eight AGCMs are run with prescribed time-
 305 evolving observed SSTs and SICs while all radiative forcing
 306 agents are varied as in the corresponding *historical* simulations.
 307 The *amip* simulations refer to the Atmospheric Model Inter-
 308 comparison Project (AMIP II) DECK experiments performed
 309 as part of CMIP6 (36); we perform our own *amip*-style sim-
 310 ulation for CESM1-CAM5. In combination with the RFMIP
 311 simulations, these simulations allow us to calculate λ and Eff-
 312 CS using regression over the period 1981-2014 as described
 313 above (see also refs. 14, 17, 19).

314 Across the eight AGCMs, the observed 1981-2014 SST trend
 315 pattern produces an average value of EffCS = 2.1°C (range
 316 1.3– 3.2°C) – in good agreement with EffCS derived from global
 317 energy budget observations (19) and implied by the observed
 318 global warming rate (Figs. 1c,d). This EffCS value is lower
 319 than the average EffCS simulated by the same coupled GCMs
 320 over 1981-2014. With identical atmospheric physics in AGCM
 321 and coupled GCM versions of each model, EffCS differences
 322 are due only to differences in observed and simulated SST and
 323 SIC trend patterns (14, 17, 19).

324 For the coupled GCMs with low values of ECS (GISS-
 325 E2-1-G, MIROC6, NorESM2-LM), 1981-2014 EffCS val-
 326 ues are similar for AGCM and coupled GCM simulations
 327 (Fig. 1c). However, for all other GCMs in our sub-
 328 set (CanESM5, CNRM-CM6-1, HadGEM3-GC31-LL, IPSL-
 329 CM6A-LR, CESM1-CAM5), 1981-2014 EffCS values in
 330 AGCMs are substantially lower than they are in the same
 331 coupled GCMs, with AGCM values being at the edge of or
 332 even below the range of EffCS values generated by internal
 333 variability in the coupled model historical simulations. This
 334 suggests that the observed SST trend pattern (Fig. 2c) reflects

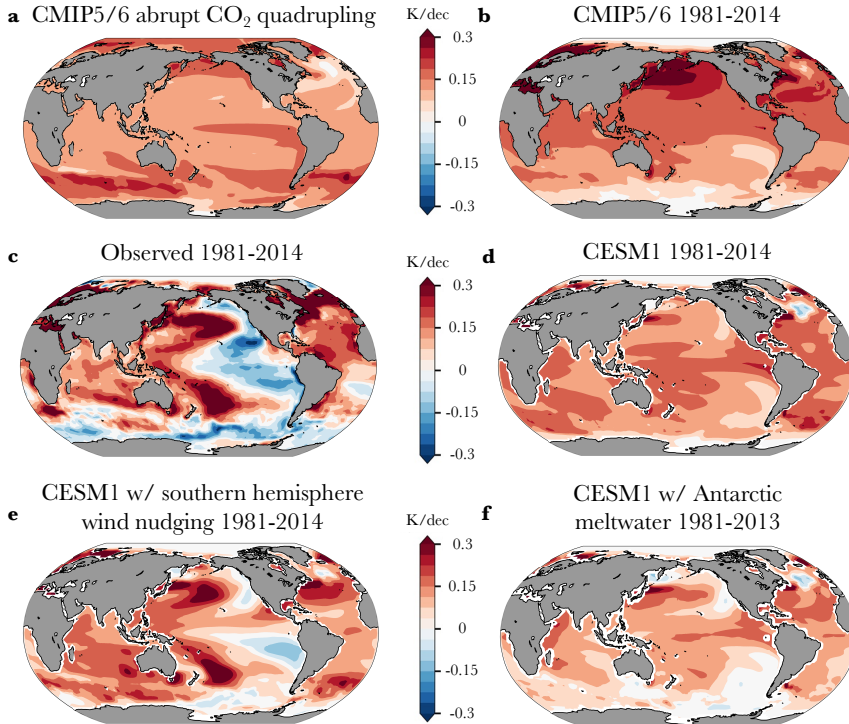


Fig. 2. Sea-surface temperature (SST) trends in CMIP5/6 models and observations. SST trend patterns for **a**, CMIP5/6 models over years 1-150 following abrupt CO_2 quadrupling (CMIP5/6 *abrupt-4xCO₂* simulation from which ECS is calculated). **b**, CMIP5/6 models over 1981-2014 (CMIP5/6 *historical* from which EffCS is calculated). **c**, Observations over 1981-2014 (from *amip*). **d**, CESM1-CAM5 over 1981-2014. **e**, CESM1-CAM5 over 1981-2014 with Southern Hemisphere high latitude wind nudging. **f**, CESM1-CAM5 over 1981-2013 with Antarctic meltwater fluxes.

an extreme phase of internal variability, a forced response not captured by the coupled GCMs, or a combination of both (17, 42). A possible reason for the larger differences between AGCM and coupled GCM values of EffCS in high-ECS models is that ECS differences across models stem largely from model differences in cloud feedbacks in the eastern tropical Pacific and Southern Oceans (35). Thus, observed cooling in these regions over 1981-2014 reduces the value of EffCS more for models with higher ECS, while leaving the value of EffCS relatively unchanged for models with lower ECS. Further examination of CESM1-CAM5 shows that the regression of local SST trends onto either the global warming trend or EffCS over 1981-2014 across ensemble members highlights the eastern tropical Pacific and Southern Oceans as key regions governing the warming rate and EffCS (Fig. S2).

The larger values of EffCS in the coupled GCMs relative to AGCMs suggests that at least a portion of the reason the coupled GCMs overestimate warming over 1981-2014 is that they fail to simulate the observed SST trend patterns – rather than simply having too-high values of ECS (or TCR). Moreover, it suggests that if the coupled GCMs were able to correctly simulate the observed warming patterns, they would produce lower values of EffCS (as shown by their AGCM simulations) and thus reduced 1981-2014 warming rates. In other words, CMIP5/6 models share a common bias in their ability to simulate the observed SST trend pattern which increases their values of EffCS and thus their rate of warming over recent decades – directly biasing their simulated relationship between warming rate and ECS on which observational constraints are based.

Correcting for SST trend pattern biases in observational constraints

We next estimate the global-mean warming each GCM would produce if it correctly simulated the observed 1981-2014 SST trend pattern. To do so, we multiply the value of EffCS derived from the AGCM simulations by the regression coefficient between the EffCS and the 1981-2014 warming rate derived from all ensemble members in the eight-GCM subset (diamonds in Fig. 1d; Methods). The results suggest that each of the eight CMIP5/6 models would have produced warming near the observed warming rate had it simulated the observed SST trend pattern. Thus, once biases in SST trend patterns are accounted for, there is little correlation between the 1981-2014 warming rate and ECS (Fig. 3a). The average warming rate correction across the eight GCMs is $-0.09^\circ\text{C dec}^{-1}$, with larger reductions in warming rates (and EffCS) for models with higher ECS (Figs. 1c and 3a).

We conclude that observed warming is consistent with a wide range of ECS values, and that by failing to account for biases in coupled GCM SST trend patterns, the proposed observational constraint biases estimates of ECS toward low values. Similar results hold if we instead use the regression between 1981-2014 EffCS and warming rate derived from each GCM separately to estimate the warming rate consistent with AGCM EffCS values, but uncertainties are larger owing to larger uncertainty in the regression, particularly for models with few ensemble members (Figs. S3-4).

As another method to estimate warming rates in the eight GCMs when correcting for biases in SST trend patterns, we use equation (3) with values of λ derived from each model's AGCM simulation (Methods). Once again, the results suggest that each of the eight CMIP5/6 models would have produced warming near the observed warming rate had they simulated the observed SST trend pattern, leaving little correlation

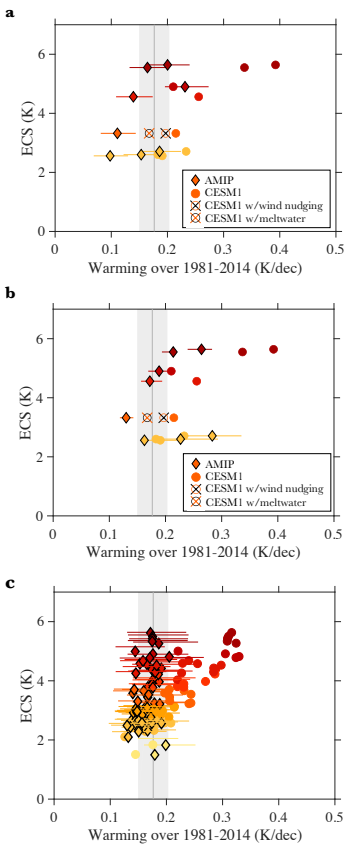


Fig. 3. Relationships between equilibrium climate sensitivity (ECS) and the 1981-2014 warming rate with (diamonds) and without (circles) accounting for observed warming patterns. ECS vs warming rate for **a**, CMIP5/6 eight-model subset, with circles showing uncorrected warming rates (from Fig. 1b) and diamonds showing corrected warming rates estimated using AGCM values of EffCS and the relationship between EffCS and warming (Fig. 1d); horizontal lines show 5–95% confidence ranges from uncertainty in the fit. **b**, CMIP5/6 eight-model subset, with circles showing uncorrected warming rates (from Fig. 1b) and diamonds showing corrected warming rates estimated using AGCM values of λ and equation (3), with horizontal lines showing uncertainty ranges reflecting the spread in κ across ensemble members. **c**, Relationship between ECS and warming rate in two-layer EBM simulations with circles showing uncorrected warming rates and diamonds showing corrected warming rates using observed values of EffCS (19) (Fig. S6), with a median of 2°C and horizontal lines showing 5–95% confidence ranges illustrating 1.5–3.1°C. Gray shading shows observational estimates (5–95% range) of observed warming rate (HadCRUT5, ref. 45).

between the 1981-2014 warming rate and ECS (Fig. 3b). The average warming rate correction across the eight GCMs is $-0.05^{\circ}\text{C dec}^{-1}$ with a larger impact for models with higher ECS, once again. This supports our conclusion that observed warming is consistent with a wide range of ECS values, and that the proposed observational constraint biases estimates of ECS toward low values; similar results hold for constraints on TCR (Figs. S1,4). It also suggests that observed global warming has been slowed by the unique SST trend pattern over recent decades (Fig. 2c) and that warming would have been more rapid had the pattern been more similar to that simulated by CMIP5/6 models (Fig. 2b).

Simulations with a two-layer energy balance model (EBM). The results presented so far rely on diagnostic interpretation of CMIP5/6 output and on inferences of GCM warming rates had they correctly simulated the observed 1981-2014

SST trend pattern and associated EffCS. Here we evaluate the robustness of this interpretation within the context of a widely-used energy balance model (EBM, refs. 54–56) which represents the Earth as two interacting layers – one representing all surface components of the climate system, including the near-surface atmosphere, ocean mixed layer, cryosphere, and land; and one representing the ocean below the mixed layer. The EBM predicts the surface temperature response to ERF through a representation of the efficiency of radiative response (governed by λ), the efficiency of ocean heat uptake, and the efficacy of ocean heat uptake which allows feedbacks to change over time as in coupled GCMs (Methods). This EBM was used extensively in IPCC AR6, including for constraining global temperature projections (see climate model “emulators” in refs. 2, 4). Here it provides a predictive physical model with all of the necessary ingredients to test the robustness of the above results derived from diagnostic analyses of CMIP5/6 models.

We fit the EBM parameters to the CMIP5/6 *abrupt4xCO₂* simulations of all models used in the analysis above (Methods; Supplementary Information). For each CMIP5/6 model parameter set, we run the EBM over the period 1850–2014 using the timeseries of historical ERF calculated as an average over the eight-model subset as described above, and we calculate EffCS over 1981–2014 using equations (1) and (2). We also run the EBM under an abrupt increase in ERF representing CO₂ quadrupling (to calculate EBM values of ECS using regression over 150 years, as in the CMIP5/6 models).

The EBM produces features similar to the CMIP5/6 analysis seen in Fig. 1. There is a strong correlation between the 1981–2014 warming rate and ECS, with lower ECS values being more consistent with observations (Figs. 3c and S5). This correlation is explained by the fact that 1981–2014 EffCS values, governing warming over that period, are similar to ECS values (Fig. S5); EffCS tends to be slightly smaller than ECS owing to the ocean heat uptake efficacy parameter being larger than one for most CMIP5/6 models (Supplementary Information), allowing feedbacks under transient warming to be slightly more negative than at equilibrium. Differences in EffCS explain a large fraction of the variance in the 1981–2014 warming rate ($r^2 = 0.88$); values of EffCS near 2°C tend to produce warming rates in line with observations, while higher values of EffCS produce too much warming (Fig. S5). The remaining variations in EBM warming rates come from differences in ocean model parameters (Methods), but differences in forcing do not contribute here because we have used the same historical ERF for all parameter sets. The regression between EffCS and the 1981–2014 warming rate also nearly matches that found from the eight-model subset, and agrees well with the relationship between EffCS and the 1981–2014 warming rate derived from observational constraints (Fig. S5).

We next consider how EBM simulations of the 1981–2014 warming rate change when we introduce a linear trend in λ (Methods), representing an idealization of trends in λ over recent decades as simulated by AGCMs forced by observed warming patterns (8, 14, 17, 19, 25), such that EffCS over 1981–2014 becomes equal to the value EffCS = 2.0°C (with bounds of 1.5 to 3.1°C also tested) estimated from global energy budget observations (19). This produces a substantial decrease in EffCS for high ECS models, but little change in EffCS for low ECS models (diamonds in Fig. S5), similar to differences seen

480 in coupled GCM and AGCM versions of CMIP5/6 models
481 (Fig. 1c). The result is that the EBM produces warming near
482 the observed rate for all CMIP5/6 model parameter sets, in
483 line with expectations based on the regression between EffCS
484 and warming rate (Figs. 3c and S5). The average warming
485 rate correction across the subset of eight models is -0.06°C
486 dec^{-1} , with larger reductions in warming rates (and EffCS)
487 for models with higher ECS, similar to our analysis using
488 CMIP5/6 models above.

489 The relationship between ECS and the warming rate when
490 imposing observed EffCS within the EBM is shown in Fig. 3c.
491 Each CMIP5/6 model parameter set produces warming near
492 the observed 1981-2014 warming rate, with little correlation
493 between warming rate and ECS. These results show that the
494 low value of EffCS produced by the observed 1981-2014 SST
495 trend pattern implies warming in line with the observed global
496 warming rate, regardless of the value of ECS. This supports
497 our interpretation that observed warming is consistent with
498 a wide range of ECS values once accounting for the observed
499 SST trend pattern and its associated low EffCS. Similar results
500 hold for comparisons of warming rates and TCR (Fig. S5).

501 **Simulations with a coupled GCM nudged toward observed**
502 **warming patterns.** Finally, we evaluate the robustness of our
503 results using two sets of CESM1-CAM5 simulations wherein
504 the coupled model is nudged toward the observed 1981-2014
505 SST trend pattern in physically-plausible ways. The first set of
506 simulations, performed by Dong et al. (57) based on methods
507 developed in Blanchard-Wrigglesworth et al. (58), involves
508 nudging Southern Hemisphere tropospheric winds (above the
509 boundary layer) poleward of 40°S to match the ERA-Interim
510 Reanalysis over the period 1981-2014; five ensemble members
511 were run, which we average together for comparison to the
512 CESM1-CAM5 ensemble mean response. The second set of
513 simulations, performed by Dong et al. (52) and Pauling et
514 al. (59), involves adding meltwater to the Southern Ocean
515 subsurface to represent discharge due to mass imbalance of the
516 Antarctic ice sheet over 1981-2013 (an effect not represented in
517 CMIP5/6 *historical* simulations); nine ensemble members were
518 run, which we average together for comparison to the CESM1-
519 CAM5 ensemble mean response. In both sets of simulations,
520 the SST trend pattern more closely matches observations, with
521 some cooling in the Southern Ocean and eastern tropical Pacific
522 Ocean and with warming in the western Pacific Ocean
523 becoming relatively larger (Figs. 2e,f); see ref. (57) for a
524 discussion of the atmospheric teleconnection pathways by which
525 these southern high latitude forcings influence tropical SST
526 patterns.

527 Using equations (1) and (2) as before, we find that both
528 sets of simulations produce smaller values of EffCS than the
529 ensemble mean of CESM1-CAM5 *historical* simulations (Fig.
530 1c), bringing EffCS nearer to that estimated from global energy
531 budget observations (19). In turn, both sets of simulations
532 show reduced global warming rates (Fig. 1d) that are more in
533 line with observations. The relationship between EffCS and
534 warming rate in these simulations also approximately follows
535 expectations based on the regression between EffCS and warming
536 rate derived from either the eight-model subset (Fig. 1d)
537 or CESM1-CAM5 (Fig. S3). However, despite similar changes
538 to EffCS, Antarctic meltwater forcing produces a larger reduction
539 in global warming rate than Southern Hemisphere wind forcing in
540 this model owing to an increase in ocean heat

541 uptake efficiency (κ) that works together with feedback (λ)
542 changes to slow the warming (52). Similar results hold for
543 comparisons of warming rates and TCR (Figs. S1,4). These
544 findings support the interpretation above that EffCS (rather
545 than ECS or TCR) governs the global warming rate over 1981-
546 2014, and that when coupled GCMs more accurately replicate
547 observed SST trend patterns, they produce lower EffCS and
548 thus slower global warming, in line with observations.

549 Discussion and conclusions

550 The results presented here suggest that high-sensitivity
551 CMIP5/6 models produce too much post-1970s warming in
552 part due to their failure to simulate observed SST trend pat-
553 terns, which in turn leads to model values of EffCS that are
554 too high compared to the observed EffCS of around 2°C over
555 this period. Because GCMs with high values of ECS and TCR
556 are able to produce values of EffCS near 2°C when forced by
557 observed SSTs over 1981-2014 (Figs. 1c, S1c), we estimate
558 that even those high-sensitivity GCMs could produce global
559 warming rates in line with observations if they were able to
560 better simulate observed SST trend patterns (Figs. 1d, 3a,b).
561 This is a bias in the GCM-based relationship between post-
562 1970s warming and climate sensitivity metrics which causes
563 the proposed observational (or “emergent”) constraint to be
564 biased toward low values of climate sensitivity. While pub-
565 lished constraints (18, 32-34) may still reflect useful lower
566 bounds on ECS and TCR, we find that they are consistent
567 with wide ranges of ECS and TCR extending to higher values
568 than previously recognized. While not a focus here, model
569 biases in historical radiative forcing (e.g., 60, 61) could also
570 impart biases in the modeled warming-sensitivity relationship
571 on which the observational constraint is based.

572 It is worth considering the implications of these results
573 for the recent climate sensitivity assessments that substantial
574 narrowed climate sensitivity uncertainty for the first time in
575 decades by estimating *very likely* ranges of around $2\text{-}5^{\circ}\text{C}$ for
576 ECS (2, 3) and $1.2\text{-}2.4^{\circ}\text{C}$ for TCR (2). That the observed rate
577 of recent warming cannot be used to constrain climate sensitiv-
578 ity means we must rely on other lines of evidence. Sherwood
579 et al. (3) employed a Bayesian framework to combine sev-
580 eral independent lines of evidence for ECS, with paleoclimate
581 observations and process understanding of climate feedbacks
582 providing strong constraints on the high end. Importantly,
583 that assessment did not use observational (or “emergent”)
584 constraints based on recent warming, so our findings do not
585 affect that assessed ECS range.

586 However, without employing a formal Bayesian framework,
587 AR6 relied on observational constraints based on global tem-
588 perature changes as the strongest constraint on the upper ends
589 of the ECS and TCR ranges (while many different lines of
590 evidence support the lower ends of the ranges). Together with
591 the recent result that the climate response to the Mt. Pinatubo
592 eruption also does not provide a reliable observational con-
593 straint on ECS (62), our findings suggest that the upper end of
594 the climate sensitivity range is less well supported than it was
595 within AR6, particularly for TCR which relied more heavily on
596 this type of observational constraint. There still remain other
597 observational constraints providing evidence against high ECS
598 values, most notably those based on proxy-estimated cooling
599 at the Last Glacial Maximum (2), but for now the Bayesian
600 framework of Sherwood et al. (3) may provide the most robust

601 support for a 2–5°C *very likely* range of ECS. A final implication
602 is that the evaluation of model ECS, TCR, and future
603 warming based on their performance in historical simulations
604 (e.g., 34, 63, 64) must also account for different sea-surface
605 temperature trend patterns between observations and models,
606 with our results suggesting that even high sensitivity models
607 are compatible with observed warming. This too suggests that
608 testing in paleoclimate settings (e.g., 65) may provide a more
609 useful evaluation of model climate sensitivity and long-term
610 warming.

611 Important questions remain, including: (i) why do CMIP5/6
612 models fail to replicate observed warming patterns over recent
613 decades, and how can this model bias be corrected? And, (ii)
614 for how long will the observed pattern of warming over recent
615 decades continue into the 21st century? Model-observation
616 discrepancies may be due to model deficiencies in simulating
617 internal variability and/or historical forced responses. Pale-
618oclimate proxy and instrumental data suggest that tropical
619 Pacific multidecadal variability may be substantially larger
620 than that produced by coupled GCMs (e.g., 66–68), which
621 seems consistent with the observed 1981–2014 SST trend pat-
622 tern resembling an extreme phase of the Interdecadal Pacific
623 Oscillation mode of variability (e.g., 41, 42, 68, 69). Alter-
624natively, several other model deficiencies have been proposed
625 to contribute to the SST trend pattern over recent decades
626 including: model biases in trends in the Southern Annular
627 Mode, potentially due to a misrepresentation of ozone deple-
628 tion (e.g., 57, 70, 71); missing Antarctic meltwater fluxes (e.g.,
629 52, 57, 59, 72); a misrepresentation of tropospheric aerosol
630 forcing, which can affect Pacific trade winds (e.g., 73); model
631 biases in Atlantic Ocean SSTs that limit the ability of the
632 Atlantic basin to affect Pacific trade winds (74); model bi-
633 ases in the transient response of the tropical Pacific to CO₂
634 forcing (e.g., 75, 76) or volcanic forcing (16); and limitations
635 associated with model resolution (e.g., 77).

636 Our findings do not depend on the source of the discrepancy
637 between CMIP5/6-simulated and observed warming patterns
638 because radiative feedbacks and EffCS depend only on SST
639 and SIC patterns, regardless of how those patterns arise (e.g.,
640 78, 79). But implicit in our use of AMIP simulations to
641 estimate how the SST trend pattern has influenced global
642 warming rates is that the pattern itself is largely independent
643 of ECS. Recent studies argue that models with more-positive
644 subtropical low-cloud feedbacks (and thus higher ECS) may
645 better replicate the observed cooling of the eastern tropical
646 Pacific (e.g., 80), at least when resulting from Southern Ocean
647 cooling (52, 57). This potential link between ECS and the
648 SST trend pattern would further support our finding that high
649 ECS models can produce low values of EffCS, and thus slow
650 global warming rates.

651 The results presented here suggest that changes in EffCS
652 have the capacity to substantially affect the global warming
653 rate and that a low value of EffCS driven by a unique SST trend
654 pattern has slowed global-mean warming over recent decades,
655 relative to what it would have been had the pattern been more
656 spatially uniform. However, more work is needed to determine
657 whether CMIP5/6 models with high ECS (above ~4°C) are
658 capable of producing the observed SST trend pattern and
659 associated low EffCS needed to bring their simulated global
660 warming rates in line with observations over recent decades.
661 It would be valuable to perform similar wind nudging and/or

662 Antarctic meltwater flux simulations, shown here for CESM1-
663 CAM5, using high ECS models.

664 These results reinforce previous findings that global warm-
665 ing will depend on how the SST trend pattern evolves in
666 the future (e.g., 52, 81–83). Our findings suggest that if the
667 observed 1981–2014 pattern continues over the 21st century,
668 then the value of EffCS governing future warming will remain
669 near 2°C. This would produce 21st century global warming
670 near the lower end of IPCC AR6 projections (Fig. S7), which
671 assume a *very likely* range of ECS of 2–5°C (2). However, if
672 enhanced warming of the eastern tropical Pacific and Southern
673 Oceans were to emerge in the future – a pattern projected
674 by GCM simulations of the 21st century and supported by
675 paleoclimate proxy evidence (e.g., 2, 84) – then EffCS would
676 increase, resulting in an increase in the rate of global warming
677 (Fig. S7). The degree to which EffCS could increase depends
678 on the magnitude of the warming in the the eastern trop-
679 ical Pacific and Southern Oceans, and on the magnitude of
680 the radiative feedbacks in those regions. Because observed
681 post-1970s warming has a unique spatial pattern that does
682 not appear to be representative of the long-term response to
683 greenhouse-gas forcing, it does not preclude the possibility that
684 high values of EffCS are possible for the future, potentially
685 leading to future warming near or even above the upper end of
686 IPCC AR6 projections if ECS turns out to be on the high end.
687 How the pattern of warming will evolve in the future thus
688 represents a major source of uncertainty in climate projections.

689 Developing improved understanding of the causes of the
690 observed SST trend pattern over recent decades and better
691 constraints on how those patterns will evolve in the future is a
692 major challenge for climate science with direct implications for
693 how we interpret the historical warming record and project 21st
694 century warming. We could, for instance, see an increase in
695 the climate's sensitivity to greenhouse-gas forcing if SST trend
696 patterns evolve to become more similar to those projected
697 by models. For now, climate model biases in historical SST
698 trend patterns suggest that caution is needed in the use of
699 models to derive observational (or “emergent”) constraints
700 on climate sensitivity or future warming based on the rate of
701 global warming over recent decades.

Materials and Methods

702

703

704 **Linear regression methods.** We use ordinary least squares (OLS)
705 regression to calculate 1981–2014 warming rates and the regression
706 of climate sensitivity metrics (ECS, TCR) against 1981–2014 warm-
707 ing rates using ensemble-mean values (Figs. 1a,b and S1a,b). To
708 estimate ECS and TCR from the warming-sensitivity relationships
709 (Figs. 1a, S1a), we calculate a linear fit of ECS (or TCR) versus
710 1981–2014 warming rate and use the parameters of that fit to esti-
711 mate ECS (or TCR) given the observed warming rate (HadCRUT5,
712 ref. 45) over 1981–2014. Uncertainties in ECS and TCR reflect
713 5–95% confidence ranges of fit parameter values.

714 For the calculation of the effective feedback λ from the regression
715 of $N - ERF$ against T (equation (1)), the presence of error in the
716 predictor variable biases OLS regression toward zero (regression
717 dilution). To correct for this, we use Deming regression, a total least
718 squares regression method, to calculate λ . We estimate the ratio
719 of error variances (variance of global average top-of-atmosphere
720 radiation and variance in global average surface temperature) to
721 be approximately $10 \text{ W}^2 \text{m}^{-4} \text{K}^{-2}$ based on AGCM simulations
722 using sea-surface temperatures fixed at pre-industrial conditions.
723 We use OLS regression for all regressions based on the two-layer

724 EBM, which does not represent internal variability. Within CESM1-
 725 CAM5, moderate correlations between EffCS and warming rate over
 726 1981–2014 are found when using the CAM5 Green's function (22)
 727 combined with SST trend patterns to estimate radiative feedback
 728 and EffCS (Fig. S2).

729 **Effective radiative forcing.** Historical effective radiative forcing
 730 (ERF) is calculated for each of the eight models in our subset
 731 using RFMIP (46) simulations. The historical ERF is diagnosed as
 732 the global top-of-atmosphere radiation anomaly in *piClim-histall*
 733 simulations (wherein SSTs and SICs are fixed to pre-industrial
 734 values while all radiative forcing agents are varied as in the corre-
 735 sponding CMIP6 *historical* simulations) relative to *piClim-control*
 736 simulations (wherein SSTs, SICs, and all radiative forcing agents
 737 are fixed to pre-industrial values). A small correction (2, 48) is
 738 made to remove the radiative response to global near-surface air
 739 temperature change T (mostly land warming) by subtracting $\lambda_{2\times}T$,
 740 where $\lambda_{2\times}$ is estimated from *abrupt4xCO₂* simulations (35). For all
 741 RFMIP simulations, the ensemble mean is used when more than one
 742 member of the simulation exist. CMIP5/6 model values of effective
 743 radiative forcing for CO₂ doubling (ERF_{2×}) have been estimated
 744 using the standard approach of extrapolating to zero global tem-
 745 perature change the regression between global top-of-atmosphere
 746 energy imbalance and global temperature change over 150 years of
 747 abrupt CO₂ quadrupling simulations, scaled by a factor of a half to
 748 account for CO₂ doubling (35, 44).

749 **Correcting for SST trend pattern biases.** For the first method of esti-
 750 mating the warming each GCM would produce if it correctly
 751 simulated the observed 1981–2014 SST trend pattern (Fig. 3a), we
 752 first calculate a linear fit (OLS regression) of EffCS versus 1981–
 753 2014 warming rate from all ensemble members of the eight-GCM
 754 subset (Fig. 1d). We then use that fit to estimate the warming
 755 rate given EffCS derived from each AGCM simulation (diamonds
 756 in Figs. 1d, 3a). Uncertainties (horizontal lines in Fig. 3a) reflect
 757 5–95% confidence ranges of fit parameter values.

758 For the second method of estimating the warming each GCM
 759 would produce if it correctly simulated the observed 1981–2014 SST
 760 trend pattern (Fig. 3b), we use equation (3) with values of λ derived
 761 from each model's AGCM simulation. In the eight-model ensemble
 762 considered here, the average correlation between λ and κ across
 763 historical ensemble members is small (average $r^2 = 0.25$), and
 764 models disagree on the sign of the correlation. Without a deeper
 765 understanding of how variations in λ and κ are related, we assume
 766 they can be varied independently and use ensemble-mean values of
 767 κ for each model in this estimate. To evaluate the degree to which
 768 variations in κ could affect the results, uncertainties (horizontal
 769 lines in Fig. 3b) are generated by using the highest and lowest values
 770 of κ from the ensemble members of each model in this calculation.

771 **Two-layer energy balance model.** The two-layer energy balance
 772 model (EBM, refs. 54–56) evolves surface temperature according to
 773 the following equations:

$$C \frac{dT}{dt} = \lambda T + \text{ERF} - \varepsilon \gamma (T - T_0), \quad [5]$$

$$C_0 \frac{dT_0}{dt} = \gamma (T - T_0),$$

774 where T is the temperature anomaly of the upper layer, represent-
 775 ing the global surface temperature anomaly; T_0 is the temperature
 776 anomaly of the lower layer; ERF is the effective radiative forcing,
 777 as above; C is the effective heat capacity of the upper layer (rep-
 778 resenting the ocean mixed layer, land, and atmosphere); C_0 is the
 779 effective heat capacity of the lower layer (representing the ocean
 780 below the mixed layer); γ represents the efficiency of vertical heat
 781 transport between upper and lower layers; and ε is the efficacy
 782 of ocean heat uptake, which allow effective radiative feedbacks to
 783 change over time as represented by coupled GCMs. Note that in
 784 the limit of $C_0 \gg C$, such that deep ocean temperature T_0 does not
 785 change much, these equations reduce to equation (3) with $\kappa = \varepsilon \gamma$.

786 We fit the two-layer EBM parameters to the *abrupt4xCO₂* sim-
 787 ulations of all CMIP5/6 models used in the analysis above using
 788 the fitting scheme developed by Lutsko and Popp (85), which was
 789 based on Geoffroy et al. (56) (see Supplementary Information for

790 parameter values). To simulate historical warming consistent with
 791 observational constraints on EffCS, we run the model using a wide
 792 range of linear trends in λ over the period 1981–2014 (starting from
 793 initial values of λ as fit to CMIP5/6 models and changing linearly
 794 with time) and calculate EffCS over this period (using equation
 795 (1)) for each. We then select the simulations that correspond to
 796 EffCS values of 2.0°C, 1.5°C, and 3.1°C (50%, 5%, and 95% inter-
 797 vals of the observationally constrained EffCS from ref. (19). See
 798 Supplementary Information for details regarding the 21st century
 799 EBM simulations under different assumptions about how EffCS will
 800 evolve in the future.

801 **ACKNOWLEDGMENTS.** KCA, CP, and LCH were supported by
 802 Department of Energy (DOE) Award DE-SC0022110, National Sci-
 803 ence Foundation (NSF) Award AGS-1752796, and National Oceanic
 804 and Atmospheric Administration (NOAA) MAPP Program Award
 805 NA20OAR4310391. KCA was supported by an Alfred P. Sloan
 806 Research Fellowship (Award FG-2020-13568) and a Calvin Profes-
 807 sorship in Oceanography. LCH was supported by the Tamaki Foun-
 808 dation. TA was supported by the Met Office Hadley Centre Climate
 809 Programme funded by BEIS and the European Union's Horizon
 810 2020 research and innovation programme under grant agreement
 811 820829. MFS was supported by NSF Award AGS-2141728. EBW
 812 was supported by NSF Award OPP-2213988. RCJW was supported
 813 by the Swiss National Science Foundation Award PCEFP2_203376
 814 and NSF Award AGS-2203543. IM was supported by NASA FI-
 815 NESST grant 80NSSC20K1657. YD was supported by the NOAA
 816 Climate and Global Change Postdoctoral Fellowship Program, ad-
 817 ministered by UCAR's Cooperative Programs for the Advancement
 818 of Earth System Science (CPAESS) under award NA210AR4310383.
 819 Work by SP was supported by the Regional and Global Model Anal-
 820 ysis Program of the Office of Science and was performed under the
 821 auspices of the U.S. Department of Energy by Lawrence Livermore
 822 National Laboratory under Contract DE-AC52-07NA27344. We also
 823 acknowledge high-performance computing support from Cheyenne
 824 (<https://doi.org/10.5065/D6RX99HX>) provided by NCAR's Com-
 825 putational and Information Systems Laboratory, sponsored by the
 826 National Science Foundation.

827 References.

1. MR Grose, J Gregory, R Coleman, T Andrews, What climate sensitivity index is most useful for projections? *Geophysical Research Letters* **45**, 1559–1566 (2018).
2. P Forster, et al., The earth's energy budget, climate feedbacks, and climate sensitivity in *In: Climate Change 2021: The Physical Science Basis. Contribution of Working Group I to the Sixth Assessment Report of the Intergovernmental Panel on Climate Change* [Masson-Delmotte, V.P. Zhai, A. Pirani, S.L. Connors, C. Peart, S. Berger, N. Caud, Y. Chen, L. Goldfarb, M. Gomis, M. Huang, K. Leitzell, E. Lonnoy, J.B.R. Matthews, T.K. Maycock, T. Waterfield, O. Yelekci, R. Yu and B. Zhou (eds.)] Cambridge University Press. (2021).
3. SC Sherwood, et al., An assessment of earth's climate sensitivity using multiple lines of evidence. *Reviews Geophysics* **58**, e2019RG000678 (2020).
4. JY Lee, et al., Future global climate: scenario-based projections and near-term information in *In: Climate Change 2021: The Physical Science Basis. Contribution of Working Group I to the Sixth Assessment Report of the Intergovernmental Panel on Climate Change* [Masson-Delmotte, V.P. Zhai, A. Pirani, S.L. Connors, C. Peart, S. Berger, N. Caud, Y. Chen, L. Goldfarb, M. Gomis, M. Huang, K. Leitzell, E. Lonnoy, J.B.R. Matthews, T.K. Maycock, T. Waterfield, O. Yelekci, R. Yu and B. Zhou (eds.)] Cambridge University Press. (2021).
5. M Collins, et al., Long-term climate change: Projections, commitments and irreversibility in *In: Climate Change 2013: The Physical Science Basis. Contribution of Working Group I to the Fifth Assessment Report of the Intergovernmental Panel on Climate Change* [Stocker, T.F., D. Qin, G.-K. Plattner, M. Tignor, S.K. Allen, J. Boschung, A. Nauels, Y. Xia, V. Bex and P.M. Midgley (eds.)]. Cambridge University Press, Cambridge, United Kingdom and New York, NY, USA. (2013).
6. A Otto, et al., Energy budget constraints on climate response. *Nature Geoscience* **6**, 415–416 (2013).
7. N Lewis, JA Curry, The implications for climate sensitivity of ar5 forcing and heat uptake estimates. *Climate Dynamics* **45**, 1009–1023 (2015).
8. JM Gregory, T Andrews, Variation in climate sensitivity and feedback parameters during the historical period. *Geophysical Research Letters* **43**, 3911–3920 (2016).
9. C Zhou, MD Zelinka, SA Klein, Impact of decadal cloud variations on the earth's energy budget. *Nature Geoscience* **9**, 871–874 (2016).
10. K Marvel, GA Schmidt, RL Miller, L Nazarenko, Implications for climate sensitivity from the response to individual forcings. *Nature Climate Change* **6**, 386–389 (2016).
11. KC Armour, Energy budget constraints on climate sensitivity in light of inconstant climate feedbacks. *Nature Climate Change* **7**, 331–335 (2017).
12. C Proistosescu, P Huybers, Energy budget constraints on climate sensitivity in light of inconstant climate feedbacks. *Science Advances* **3** (2017).

865 13. N Lewis, J Curry, The impact of recent forcing and ocean heat uptake data on estimates of
866 climate sensitivity. *Journal Climate* **3**, 6051–6071 (2018).

867 14. T Andrews, et al., Accounting for changing temperature patterns increases historical estimates of climate sensitivity. *Geophysical Research Letters* **45** (2018).

868 15. K Marvel, R Pincus, GA Schmidt, RL Miller, Implications for climate sensitivity from the response to individual forcings. *Geophysical Research Letters* **45**, 1595–1601 (2018).

871 16. JM Gregory, T Andrews, P Ceppi, T Mauritsen, MJ Webb, How accurately can the climate sensitivity to CO₂ be estimated from historical climate change? *Climate Dynamics* **54**, 129–157 (2020).

874 17. Y Dong, et al., Biased estimates of equilibrium climate sensitivity and transient climate response derived from historical cmip6 simulations. *Geophysical Research Letters* **48**, e2021GL095778 (2021).

876 18. M Winton, et al., Climate sensitivity of gfdl's cm4.0. *Journal Advances Modeling Earth Systems* **12**, e2019M0S01838 (2020).

878 19. T Andrews, et al., On the effect of changing sst patterns on historical radiative feedbacks. *Journal Geophysical Research: Atmospheres* **127** (2022).

880 20. KC Armour, CM Bitz, GH Roe, Time-varying climate sensitivity from regional feedbacks. *Journal Climate* **26**, 4518–4534 (2013).

882 21. T Andrews, JM Gregory, MJ Webb, The dependence of radiative forcing and feedback on evolving patterns of surface temperature change in climate models. *Journal Climate* **28**, 1630–1648 (2015).

884 22. C Zhou, MD Zelinka, SA Klein, Analyzing the dependence of global cloud feedback on the spatial pattern of sea surface temperature change with a green's function approach. *Journal Advances Modeling Earth Systems* **9**, 2174–2189 (2017).

886 23. P Ceppi, JM Gregory, Relationship of tropospheric stability to climate sensitivity and earth's observed radiation budget. *Proceedings National Academy Sciences* **114**, 13126–13131 (2017).

888 24. T Andrews, MJ Webb, The dependence of global cloud and lapse rate feedbacks on the spatial structure of tropical pacific warming. *Journal Climate* **31**, 641–654 (2018).

890 25. Y Dong, C Proistosescu, KC Armour, DS Battisti, Attributing historical and future evolution of radiative feedbacks to regional warming patterns using a green's function approach: The preeminence of the western pacific. *Journal Climate* **32**, 5471–5491 (2019).

892 26. Y Dong, et al., Intermodel spread in the pattern effect and its contribution to climate sensitivity in cmip5 and cmip6 models. *Journal Climate* **33**, 7755–7775 (2020).

894 27. S Fuglestater, LG Silvers, The peculiar trajectory of global warming. *Journal Geophysical Research: Atmospheres* **126**, e2020JD033629 (2021).

896 28. SA Klein, A Hall, Emergent constraints for cloud feedbacks. *Current Climate Change Reports* **1**, 276–287 (2015).

900 29. A Hall, P Cox, C Huntington, S Klein, Progressing emergent constraints on future climate change. *Nature Climate Change* **9**, 269–278 (2019).

902 30. V Eyring, et al., Taking climate model evaluation to the next level. *Nature Climate Change* **9**, 102–110 (2019).

904 31. F Brant, The potential for structural errors in emergent constraints. *Advances Atmospheric Sciences* **37**, 1–15 (2020).

906 32. D Jiménez-de-la Cuesta, , T Mauritsen, Emergent constraints on earth's transient and equilibrium response to doubled CO₂ from post-1970s global warming. *Nature Geoscience* **12**, 902–905 (2019).

908 33. FJMM Nijssse, PM Cox, MS Williamson, An emergent constraint on transient climate response from simulated historical warming in cmip6 models. *Earth System Dynamics* **11**, 737–750 (2020).

910 34. KB Tokarska, et al., Past warming trend constrains future warming in cmip6 models. *Science Advances* **12** (2020).

912 35. MD Zelinka, et al., Causes of higher climate sensitivity in cmip6 models. *Geophysical Research Letters* **47**, e2019GL085782 (2020).

914 36. V Eyring, et al., Overview of the coupled model intercomparison project phase 6 (cmip6) experimental design and organization. *Geoscientific Model Development* **9**, 1937–1958 (2016).

916 37. Z Hausfather, K Marvel, GA Schmidt, JW Nielsen-Gammon, M Zelinka, Climate simulations: recognize the 'hot model' problem. *Nature* **605**, 26–29 (2022).

918 38. PM Caldwell, et al., Statistical significance of climate sensitivity predictors obtained by data mining. *Geophysical Research Letters* **41**, 1803–1808 (2014).

920 39. PM Caldwell, MD Zelinka, SA Klein, Evaluating emergent constraints on equilibrium climate sensitivity. *Journal Climate* **31**, 3921–3942 (2018).

922 40. BM Sanderson, et al., The potential for structural errors in emergent constraints. *Earth Syst. Dynam.* **12**, 899–918 (2021).

924 41. S McGregor, et al., Recent walker circulation strengthening and pacific cooling amplified by atlantic warming. *Nature Climate Change* **4**, 888–892 (2014).

926 42. RCJ Wills, Y Dong, C Proistosescu, KC Armour, DS Battisti, Systematic climate model biases in the large-scale patterns of recent sea-surface temperature and sea-level pressure change. *Geophysical Research Letters* **49** (2022).

928 43. C Smith, et al., The earth's energy budget, climate feedbacks, and climate sensitivity supplementary material in *In: Climate Change 2021: The Physical Science Basis. Contribution of Working Group I to the Sixth Assessment Report of the Intergovernmental Panel on Climate Change [Masson-Delmotte, V, P Zhai, A Pirani, SL Connors, C Pearn, S Berger, N Caud, Y Chen, L Goldfarb, M Gomis, M Huang, K Leitzell, E Lonnoy, JBR Matthews, TK Maycock, T Waterfield, O Yelekci, R Yu and B Zhou (eds.)] Cambridge University Press.* (2021).

930 44. I Mitevski, PL M, C Orbe, Asymmetric warming/cooling response to CO₂ increase/decrease mainly due to non-logarithmic forcing, not feedbacks. *Geophysical Research Letters* **49**, e2021GL097133 (2022).

932 45. CP Morice, et al., An updated assessment of near-surface temperature change from 1850: The hadcrut5 data set. *Journal Geophysical Research: Atmospheres* **126**, e2019JD032361 (2021).

934 46. R Pincus, PM Forster, B Stevens, The radiative forcing model intercomparison project (rfmip): experimental protocol for cmip6. *Geoscientific Model Development* **9**, 3447–3460 (2016).

936 47. T Andrews, et al., Effective radiative forcing in a gcm with fixed surface temperatures. *Journal Geophysical Research: Atmospheres* **126**, e2020JD033880 (2021).

938 48. J Hansen, et al., Efficacy of climate forcings. *Journal Geophysical Research: Atmospheres* **110**, D18104 (2005).

940 49. JM Gregory, MJF B, The climate response to CO₂ of the hadley centre coupled aogcm with and without flux adjustment. *Geophysical Research Letters* **24**, 1943–1946 (1997).

942 50. JM Gregory, MJF B, The role of climate sensitivity and ocean heat uptake on aogcm transient temperature response. *Journal Climate* **15**, 124–130 (2002).

944 51. JM Gregory, T Andrews, P Good, The inconstancy of the transient climate response parameter under increasing CO₂. *Philosophical Transactions Royal Society A* **373**, 20140417 (2015).

946 52. Y Dong, A Pauling, S Sadai, KC Armour, Antarctic ice-sheet meltwater reduces transient warming and climate sensitivity through the sea-surface temperature pattern effect. *Geophysical Research Letters* **49** (2022).

948 53. RP Allan, et al., Changes in global net radiative imbalance 1985?2012. *Geophysical Research Letters* **41**, 5588–5597 (2014).

950 54. JM Gregory, Vertical heat transports in the ocean and their effect on time-dependent climate change. *Climate Dynamics* **16**, 501–515 (2000).

952 55. IM Held, et al., Probing the fast and slow components of global warming by returning abruptly to preindustrial forcing. *Journal Climate* **23**, 2418–2427 (2010).

954 56. O Geoffroy, et al., Transient climate response in a two-layer energy-balance model. part ii: Representation of the efficacy of deep-ocean heat uptake and validation for cmip5 aogcms. *Journal Climate* **26**, 1859–1876 (2013).

956 57. Y Dong, KC Armour, DS Battisti, E Blanchard-Wrigglesworth, Two-way teleconnections between the southern ocean and the tropical pacific via a dynamic feedback. *Journal Climate* **35**, 2667–2682 (2022).

958 58. E Blanchard-Wrigglesworth, LA Roach, A Donohoe, Q Ding, Impact of winds and southern ocean ssts on antarctic sea ice trends and variability. *Journal Climate* **34**, 949–965 (2021).

960 59. AG Pauling, CM Bitz, IJ Smith, PJ Langhorne, The response of the southern ocean and antarctic sea ice to freshwater from ice shelves in an earth system model. *Journal Climate* **29**, 1655–1672 (2016).

962 60. CJ Smith, PM Forster, Suppressed late-20th century warming in cmip6 models explained by forcing and feedbacks. *Geophysical Research Letters* **48** (2021).

964 61. JT Fasullo, et al., Spurious late historical-era warming in cesm2 driven by prescribed biomass burning emissions. *Geophysical Research Letters* **49** (2022).

966 62. AG Pauling, CM Bitz, KC Armour, The climate response to the mt. pinatubo eruption does not constrain climate sensitivity. *Geophysical Research Letters* **50** (2023).

968 63. Y Liang, NP Gillett, AH Monahan, Climate model projections of 21st century global warming-constrained using the observed warming trend. *Geophysical Research Letters* **47** (2020).

970 64. A Ribes, S Qasmi, NP Gillett, Making climate projections conditional on historical observations. *Science Advances* **7** (2021).

972 65. J Zhu, et al., Assessment of equilibrium climate sensitivity of the community earth system model version 2 through simulation of the last glacial maximum. *Geophysical Research Letters* **48** (2021).

974 66. T Laepple, P Huybers, Global and regional variability in marine surface temperatures. *Geophysical Research Letters* **41**, 2528–2534 (2014).

976 67. T Laepple, P Huybers, Ocean surface temperature variability: Large model–data differences at decadal and longer periods. *Proceedings National Academy Sciences* **111**, 16682–16687 (2014).

978 68. BJ Henley, et al., Spatial and temporal agreement in climate model simulations of the inter-decadal pacific decadal oscillation. *Environmental Research Letters* **12**, 044011 (2017).

980 69. S Po-Chedley, et al., Natural variability contributes to model–satellite differences in tropical tropospheric warming. *Proceedings National Academy Sciences* **118** (2021).

982 70. Y Kostov, D Ferreira, KC Armour, J Marshall, Contributions of greenhouse gas forcing and the southern annular mode to historical southern ocean surface temperature trends. *Geophysical Research Letters* **45**, 1086–1097 (2018).

984 71. DL Hartmann, The antarctic ozone hole and the pattern effect on climate sensitivity. *Proceedings National Academy Sciences* **35** (2022).

986 72. A Purich, MH England, W Cai, A Sullivan, PJ Durack, Impacts of broad-scale surface freshening of the southern ocean in a coupled climate model. *Journal Climate* **31**, 2613–2632 (2018).

988 73. C Takahashi, M Watanabe, Pacific trade winds accelerated by aerosol forcing over the past two decades. *Nature Climate Change* **6**, 768–772 (2016).

990 74. S McGregor, MF Steecker, JB Kaitar, MH England, M Collins, Model tropical atlantic biases underpin diminished pacific decadal variability. *Nature Climate Change* **8**, 493–498 (2018).

992 75. T Kohyama, DL Hartmann, DS Battisti, La niña-like mean-state response to global warming and potential oceanic roles. *Journal Climate* **30**, 4207–4225 (2017).

994 76. R Seager, et al., Strengthening tropical pacific zonal sea surface temperature gradient consistent with rising greenhouse gases. *Nature Climate Change* **9**, 517–522 (2019).

996 77. T Rackow, et al., Delayed antarctic sea-ice decline in high-resolution climate change simulations. *Nature Communications* **13** (2023).

998 78. AD Haugstad, KC Armour, DS Battisti, BEJ Rose, Relative roles of surface temperature and climate forcing patterns in the inconstancy of radiative feedbacks. *Geophysical Research Letters* **44** (2017).

1000 79. M Zhou, C Wang, MD Zelinka, Y Liu, Y Dong, AK C, Explaining forcing efficacy with pattern effect and state dependence. *Geophysical Research Letters* **50** (2023).

1002 80. H Kim, SM Kang, JE Kay, SP Xie, Subtropical clouds key to southern ocean teleconnections to the tropical pacific. *Proceedings National Academy Sciences* **119** (2022).

1004 81. WR Frey, EA Maroon, AG Pendergrass, JE Kay, Do southern ocean cloud feedbacks matter for 21st century warming? *Geophysical Research Letters* **11**, 33–37 (2017).

1006 82. M Watanabe, JL Dufresne, Y Kosaka, T Mauritsen, T Hiroaki, Enhanced warming constrained by past trends in equatorial pacific sea surface temperature gradient. *Nature Climate Change* **11**, 33–37 (2021).

1008 83. A Gjermundsen, et al., Shutdown of southern ocean convection controls long-term greenhouse gas-induced warming. *Nature Geoscience* **14**, 724–731 (2021).

1033 84. JE Tierney, AM Haywood, R Fend, T Bhattacharya, BL Otto-Btiesner, Pliocene warmth con-
1034 sistent with greenhouse gas forcing. *Geophysical Research Letters* **46** (2019).

1035 85. NJ Lutsko, M Popp, Probing the sources of uncertainty in transient warming on different
1036 timescales. *Geophysical Research Letters* **46**, 11367–11377 (2019).

DRAFT

1

2 **Supplementary Information for**

3 **Sea-surface temperature pattern effects have slowed global warming and biased 4 warming-based constraints on climate sensitivity**

5 **Kyle C. Armour, Cristian Proistosescu, Yue Dong, Lily C. Hahn, Edward Blanchard-Wrigglesworth, Andrew G. Pauling, Robert
6 C. Jnglin Wills, Timothy Andrews, Malte F. Stuecker, Stephen Po-Chedley, Ivan Mitevski, Piers M. Forster, and Jonathan M.
7 Gregory**

8 **Kyle Armour**
9 **E-mail:** karmour@uw.edu

10 **This PDF file includes:**

11 Supplementary text
12 Figs. S1 to S7
13 Tables S1 to S2

14 **Supporting Information Text**

15 **Tables S1 and S2**

16 Tables S1 and S2 show relevant parameters for CMIP5 and CMIP6 models, respectively. This includes the number of *historical*
17 ensemble members used in the analysis in the main text; equilibrium climate sensitivity (ECS); transient climate response
18 (TCR); and two-layer energy balance model (EBM) parameter values. Also noted are which models are included in our
19 eight-model subset.

20 **The relationship between post-1970s warming rate and transient climate response**

21 Fig. S1 shows the equivalent of Fig. 1 in the main text, but for the relationship between TCR and the 1981-2014 warming rate
22 or effective climate sensitivity (EffCS). TCR values are calculated from the global temperature change near year 70 (time of
23 CO₂ doubling) of CMIP5/6 1%/yr CO₂ ramping simulations (*1pctCO₂*). See Fig. S4 for the relationships between TCR and
24 the 1981-2014 warming rate when accounting for observed sea-surface temperature (SST) trend patterns.

25 **The relationship between SST trend patterns, EffCS, and global warming rate in the CESM1-CAM5 large ensemble**

26 Fig. S2 shows regressions between local SST trend patterns and either global warming rates or EffCS over 1981-2014. Also
27 shown is the relationship between EffCS and warming rate over 1981-2014 when using the CAM5 Green's function of Zhou et
28 al. (22) combined with SST trend patterns to estimate radiative feedback and EffCS (Fig. S2c), rather than regression methods
29 as in Fig. 1d of the main text.

30 **Correcting for warming rates using model-specific relationships between EffCS and warming rates over 1981-2014**

32 Figs. S3 and S4c,d show the equivalent of Figs. 1d and 3a in the main text, but using model-specific relationships between
33 EffCS and warming rates over 1981-2014 in the estimate of the warming rate in each model had it simulated the observed SST
34 trend pattern.

35 **Two-layer energy balance model (EBM) simulations**

36 Figure S5 shows the equivalent of Fig. 1 in the main text, but for the EBM response to historical (to 2014) and RCP8.5 (to
37 2100) ERF as described in the Methods. Figure S7a shows the EBM response to historical and RCP8.5 ERF over 1850-2100
38 using parameters fit to CMIP5/6 models (see Methods, and Tables S1-2). We also run the EBM under a linear increase in ERF
39 representing 1%/yr CO₂ ramping simulations (to calculate EBM values of TCR, as in the CMIP5/6 models).

40 Figure S6a shows EffCS within the EBM, illustrating that EffCS values are near ECS values for each ensemble member.
41 EffCS is calculated from the linear regression of global radiative response and global surface warming (Methods) within
42 running 34-year windows (the length of the period 1981-2014), and EffCS values vary over time depending on the degree of
43 disequilibrium between the upper and lower ocean layers owing to the efficacy of ocean heat uptake parameter (Methods). To
44 illustrate the impact of changing EffCS on projected warming, we introduce a linear trend in the radiative feedback λ such that
45 EffCS $\approx 2^{\circ}\text{C}$ over the period 1981-2014 for each CMIP5/6 parameter set (Fig. S6b), with this value of EffCS chosen to match
46 observed energy budget constraints and *amip* simulations (see main text). This produces the 1981-2014 warming rates shown
47 by the diamonds in Fig. S5 and Fig. 3c.

48 We also perform several extensions of these simulations with various hypothetical evolutions of λ and EffCS over the period
49 2015-2100. We consider three scenarios: (i) λ remains constant over the period 2015-2100, thus maintaining EffCS $\approx 2^{\circ}\text{C}$
50 (Fig. S6b); (ii) λ is linearly returned to CMIP5/6 model values by 2050 (reversing the linear λ trend applied over 1981-2014
51 in approximately the same number of years) (Fig. S6c); and (iii) λ is linearly returned to CMIP5/6 model values by 2100
52 (reversing the linear λ trend applied over 1981-2014 but more slowly) (Fig. S6d). Figure S7 shows the EBM temperature
53 response in each of these scenarios.

Table S1. CMIP5 model ECS, TCR, and two-layer energy balance model (EBM) parameter values. Number of *historical* ensemble members used in the analysis listed in parentheses. Models included in the eight-model subset in the main text denoted by *.

Model	Two-layer EBM parameters fit to <i>abrupt4xCO₂</i> simulations							
	ECS (K)	TCR (K)	C (W yr m ⁻² K ⁻¹)	C_0 (W yr m ⁻² K ⁻¹)	λ (Wm ⁻² K ⁻¹)	γ (Wm ⁻² K ⁻¹)	ε	ERF _{2×} (Wm ⁻²)
ACCESS1-0 (1)	3.90	1.77	8.9	83	-0.81	0.71	1.55	3.6
ACCESS1-3 (1)	3.63	1.60	10.1	114	-0.81	0.72	1.62	3.5
bcc-csm1-1 (1)	2.91	1.76	8.8	57	-1.28	0.58	1.27	3.6
CCSM4 (6)	2.94	1.80	7.8	72	-1.40	0.81	1.36	4.2
CESM1-CAM5* (40)	3.32	2.07	8.7	144	-1.22	0.60	1.19	4.3
CNRM-CM5 (1)	3.28	1.97	8.7	96	-1.12	0.51	0.92	3.5
CSIRO-Mk3-6-0 (10)	4.36	1.69	9.3	77	-0.66	0.71	1.80	3.4
CanESM2 (5)	3.71	2.30	8.3	77	-1.05	0.54	1.28	4.1
GFDL-CM3 (3)	4.03	1.76	9.9	76	-0.78	0.71	1.39	3.4
GFDL-ESM2G (1)	2.34	1.21	6.5	104	-1.48	0.80	1.17	3.5
GFDL-ESM2M (1)	2.46	1.37	8.9	113	-1.38	0.86	1.23	3.6
GISS-E2-H (5)	2.43	1.78	10.5	86	-1.64	0.70	1.27	4.1
GISS-E2-R (6)	2.28	1.48	6.1	135	-2.03	1.07	1.44	4.6
HadGEM2-ES (4)	4.64	2.43	8.3	99	-0.60	0.49	1.57	3.4
inmcm4 (1)	2.05	1.29	9.1	277	-1.57	0.69	1.82	3.0
IPSL-CM5A-LR (4)	4.05	1.97	8.6	100	-0.79	0.57	1.14	3.3
IPSL-CM5B-LR (1)	2.64	1.44	9.7	68	-1.07	0.63	1.43	3.0
MIROC5 (5)	2.70	1.47	9.7	163	-1.58	0.74	1.20	4.4
MPI-ESM-LR (3)	3.66	2.01	9.2	78	-1.20	0.62	1.43	4.7
MRI-CGCM3 (1)	2.61	1.52	10.1	70	-1.30	0.60	1.25	3.5
NorESM1-M (1)	2.93	1.39	9.9	122	-1.15	0.76	1.57	3.6

Table S2. CMIP6 model ECS, TCR, and two-layer energy balance model (EBM) parameter values. Number of *historical* ensemble members used in the analysis listed in parentheses. Models included in the eight-model subset in the main text denoted by *.

Model	Two-layer EBM parameters fit to <i>abrupt4xCO₂</i> simulations							
	ECS (K)	TCR (K)	C (W yr m ⁻² K ⁻¹)	C_0 (W yr m ⁻² K ⁻¹)	λ (Wm ⁻² K ⁻¹)	γ (Wm ⁻² K ⁻¹)	ε	ERF _{2×} (Wm ⁻²)
ACCESS-CM2 (3)	4.72	2.10	9.0	93	-0.71	0.53	1.55	4.0
ACCESS-ESM1-5 (20)	3.87	1.95	9.0	97	-0.72	0.60	1.73	3.5
AWI-CM-1-1-MR (5)	3.16	2.06	8.3	57	-1.22	0.46	1.49	4.1
BCC-CSM2-MR (3)	3.02	1.72	6.5	64	-1.20	0.84	1.37	3.8
BCC-ESM1 (3)	3.26	1.77	8.9	98	-0.91	0.52	1.39	3.3
CAMS-CSM1-0 (7)	2.29	1.73	10.2	61	-1.87	0.47	1.29	4.4
CanESM5* (25)	5.64	2.74	8.0	80	-0.65	0.52	1.07	3.8
CESM2 (11)	5.15	2.06	8.7	75	-0.69	0.66	1.89	4.5
CESM2-WACCM (3)	4.68	1.98	8.5	89	-0.74	0.69	1.57	4.1
CMCC-CM2-SR5 (1)	3.52	2.09	8.9	79	-1.06	0.41	1.27	4.0
CNRM-CM6-1* (30)	4.90	2.14	7.6	147	-0.74	0.50	1.00	3.6
CNRM-CM6-1-HR (1)	4.33	2.48	8.2	95	-0.92	0.55	0.72	3.7
CNRM-ESM2-1 (10)	4.79	1.86	7.5	100	-0.63	0.59	0.91	2.9
E3SM-1-0 (3)	5.31	2.99	8.6	44	-0.63	0.35	1.50	3.7
EC-Earth3 (73)	4.10	2.30	8.1	37	-0.81	0.42	1.42	3.7
EC-Earth3-Veg (8)	4.33	2.62	8.4	40	-0.82	0.40	1.42	3.8
FGOALS-f3-L (3)	2.98	1.94	9.3	88	-1.41	0.53	1.58	4.7
FGOALS-g3 (5)	2.88	1.54	7.8	98	-1.30	0.69	1.30	4.0
GISS-E2-1-G* (12)	2.71	1.80	6.7	144	-1.47	0.84	1.10	4.1
GISS-E2-1-H (25)	3.12	1.93	8.9	86	-1.15	0.61	1.20	3.7
HadGEM3-GC31-LL* (5)	5.55	2.55	8.0	77	-0.63	0.51	1.22	3.7
HadGEM3-GC31-MM (4)	5.42	2.58	8.3	73	-0.66	0.58	1.03	3.6
INM-CM4-8 (1)	1.83	1.33	6.4	26	-1.68	0.78	1.31	3.1
IPSL-CM6A-LR* (32)	4.56	2.32	8.2	63	-0.75	0.41	1.33	3.7
KACE-1-0-G (3)	4.48	1.41	9.0	120	-0.71	0.74	1.31	3.8
MIROC-ES2L (11)	2.66	1.55	10.6	185	-1.56	0.67	0.93	4.1
MIROC6* (50)	2.60	1.55	8.9	175	-1.38	0.65	1.32	3.9
MPI-ESM1-2-HAM (3)	2.96	1.80	9.5	113	-1.44	0.64	1.34	4.5
MPI-ESM1-2-HR (8)	2.98	1.66	8.9	84	-1.33	0.66	1.50	4.3
MPI-ESM1-2-LR (10)	3.00	1.84	9.5	114	-1.40	0.59	1.23	4.4
MRI-ESM2-0 (6)	3.13	1.64	8.7	96	-1.21	0.85	1.43	4.1
NESM3 (5)	4.77	2.72	5.6	105	-0.78	0.46	0.97	3.7
NorCPM1 (29)	3.05	1.56	9.9	108	-1.18	0.78	1.55	4.0
NorESM2-LM* (3)	2.56	1.48	5.6	119	-1.71	0.86	1.99	5.0
NorESM2-MM (3)	2.50	1.33	6.0	114	-1.74	0.79	1.66	4.8
SAM0-UNICON (1)	3.72	2.27	7.3	100	-1.09	0.79	1.24	4.3
TaiESM1 (1)	4.31	2.34	8.8	97	-0.93	0.63	1.34	4.4
UKESM1-0-LL (18)	5.36	2.79	8.0	80	-0.67	0.52	1.12	3.7

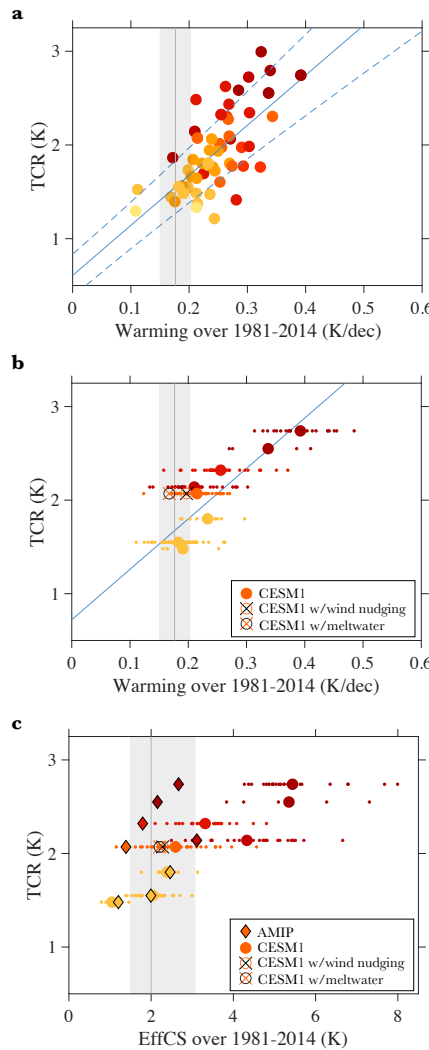


Fig. S1. Relationships between transient climate response (TCR), effective climate sensitivity (EffCS), and the 1981-2014 warming rate in CMIP5/6 models. **a**, CMIP5/6 TCR versus warming rate using averages of all available ensemble members for each model ($r^2 = 0.46$); colors correspond to values of ECS. **b**, Eight-model subset TCR versus warming rate with ensemble means shown as larger circles and ensemble members shown as smaller dots. **c**, Eight-model subset TCR versus EffCS over 1981-2014 with ensemble means shown as larger circles and ensemble members shown as smaller dots; diamonds show EffCS values from AGCM simulations forced by observed SST trend patterns. In **b,c**, open circles show CESM1-CAM5 simulations with wind nudging or meltwater forcing as described in the main text. Blue lines show fits calculated using ordinary least squares regression, with dashed blue lines showing 5-95% ranges of fit parameters. Gray shading shows observational estimates (5-95% range) of observed warming rate and EffCS as described in the main text.

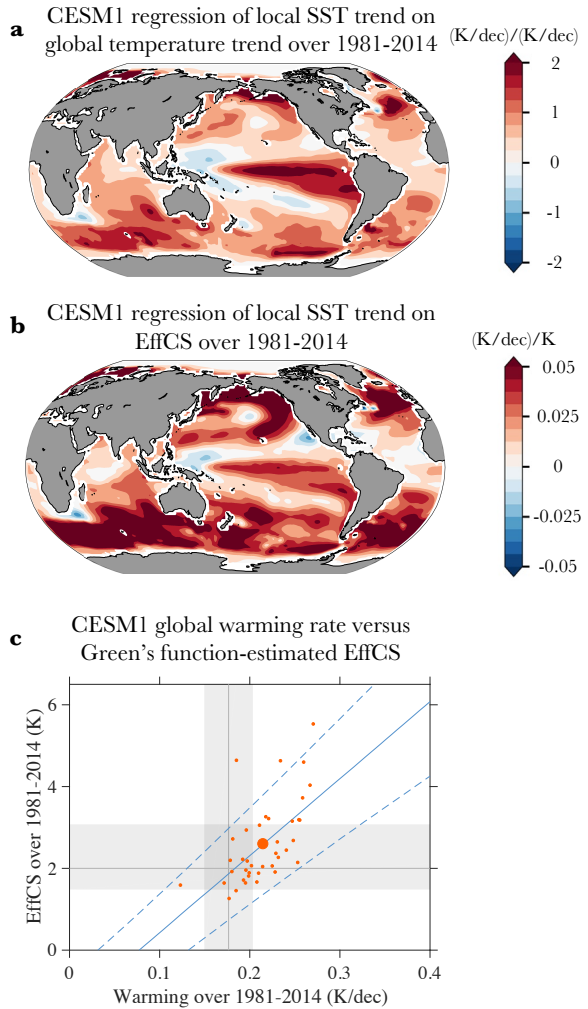


Fig. S2. The relationship between SST trend patterns, EffCS, and 1981-2014 warming rate in the CESM1 large ensemble. **a**, Regression between local SST trends and global warming rates across ensemble members. **b**, Regression between local SST trends and EffCS values (calculated as described in main text) across ensemble members. **c**, Green's function-estimated EffCS (calculated using the CAM5 Green's function of Zhou et al. (22) convolved with SST trend pattern of each ensemble member) versus warming rate over 1981-2014, with ensemble mean shown as larger circles and ensemble members shown as smaller dots ($r^2 = 0.36$). Blue lines show fit calculated using ordinary least squares regression, with dashed blue lines showing 5-95% ranges of fit parameters. Gray shading shows observational estimates (5-95% range) of observed warming rate and EffCS as described in the main text.

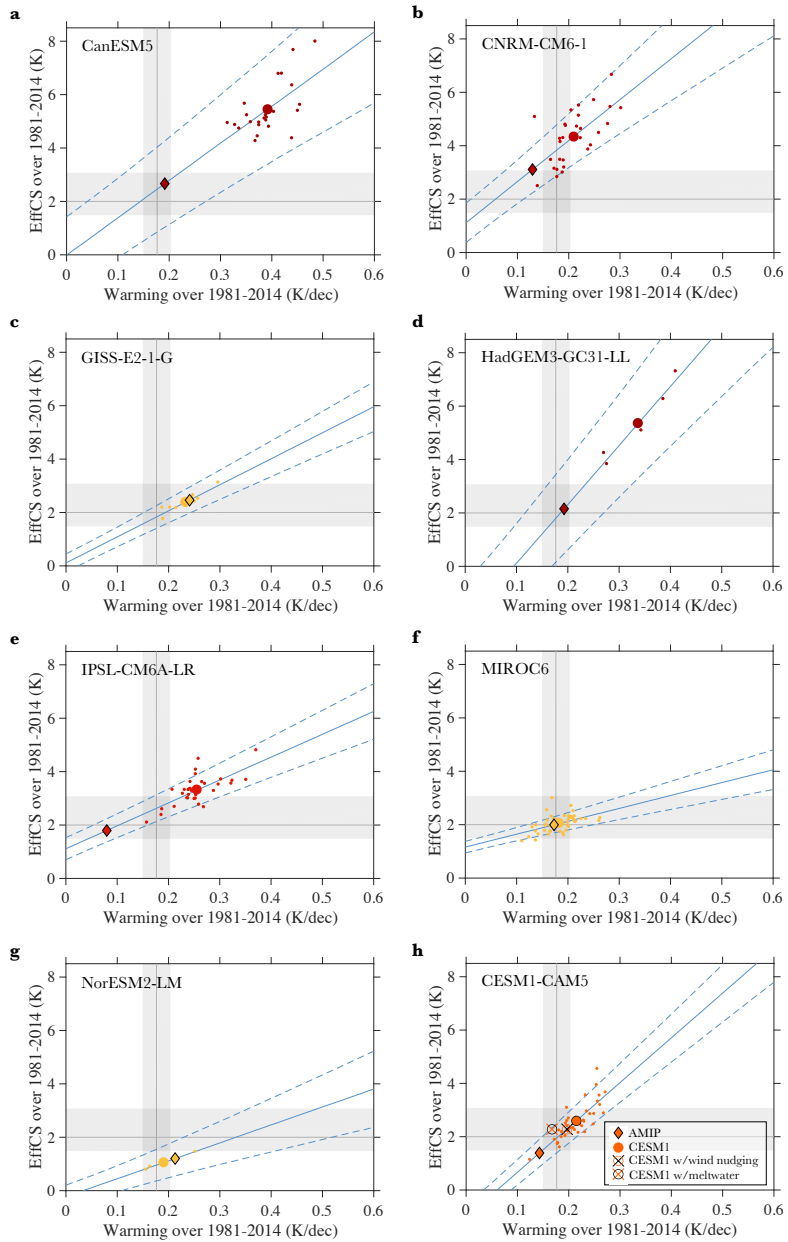


Fig. S3. Relationships between effective climates sensitivity (EffCS) over 1981-2014 and 1981-2014 warming rate in individual CMIP5/6 models. **a**, CanESM5. **b**, CNRM-CM6-1. **c**, GISS-E2-1-G. **d**, HadGEM3-CG3-LL. **e**, IPSL-CM6A-LR. **f**, MIROC6. **g**, NorESM2-LM. **h**, CESM1-CAM5. Ensemble means shown as larger circles and ensemble members shown as smaller dots. Also shown are EffCS and warming rates in CESM1-CAM5 simulations with wind nudging or meltwater forcing (see main text). Blue lines show fits calculated using ordinary least squares regression, with dashed blue lines showing 5-95% ranges of fit parameters. Gray shading shows observational estimates (5-95% range) of observed warming rate (HadCRUT5) and EffCS (see main text). Diamonds show EffCS values from AGCM simulations forced by observed warming patterns, with the corresponding warming rates estimated from the regression between EffCS over 1981-2014 and warming rate for each model.

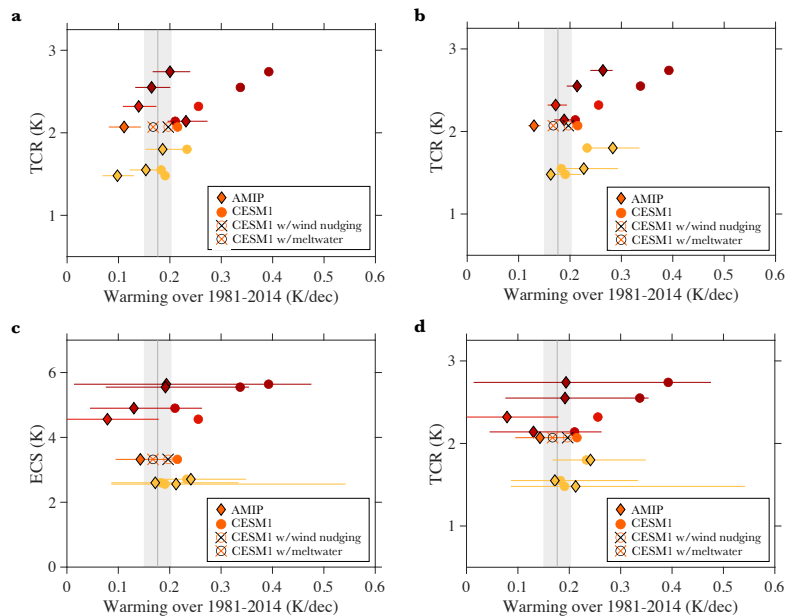


Fig. S4. Relationships between climate sensitivity metrics and the 1981-2014 warming rate with (diamonds) and without (circles) accounting for observed warming patterns. TCR vs warming rate for **a**, CMIP5/6 eight-model subset, with circles showing uncorrected warming rates (from Fig. 1b) and diamonds showing corrected warming rates estimated using AGCM values of EffCS and the relationship between EffCS and warming (Fig. 1d); horizontal lines show 5-95% confidence ranges from uncertainty in the fit. **b**, CMIP5/6 eight-model subset, with circles showing uncorrected warming rates (Fig. S1b) and diamonds showing corrected warming rates estimated using AGCM values of λ and equation (3), with horizontal lines showing uncertainty ranges reflecting the spread in κ across ensemble members. **c**, CMIP5/6 ECS vs warming rate, with corrected warming rates (diamonds) estimated using AGCM values of EffCS and the relationship between EffCS and warming in the individual CMIP5/6 models (Fig. S3), with horizontal lines showing 5-95% confidence ranges from uncertainty in the fit; circles show uncorrected values as in Fig. 1b. **d**, CMIP5/6 TCR vs warming rate, with corrected warming rates (diamonds) estimated using AGCM values of EffCS and the relationship between EffCS and warming in the individual CMIP5/6 models (Fig. S2), with horizontal lines showing 5-95% confidence ranges from uncertainty in the fit; circles show uncorrected values as in Fig. S1b. Gray shading shows observational estimates (5-95% range) of observed warming rate as described in the main text.

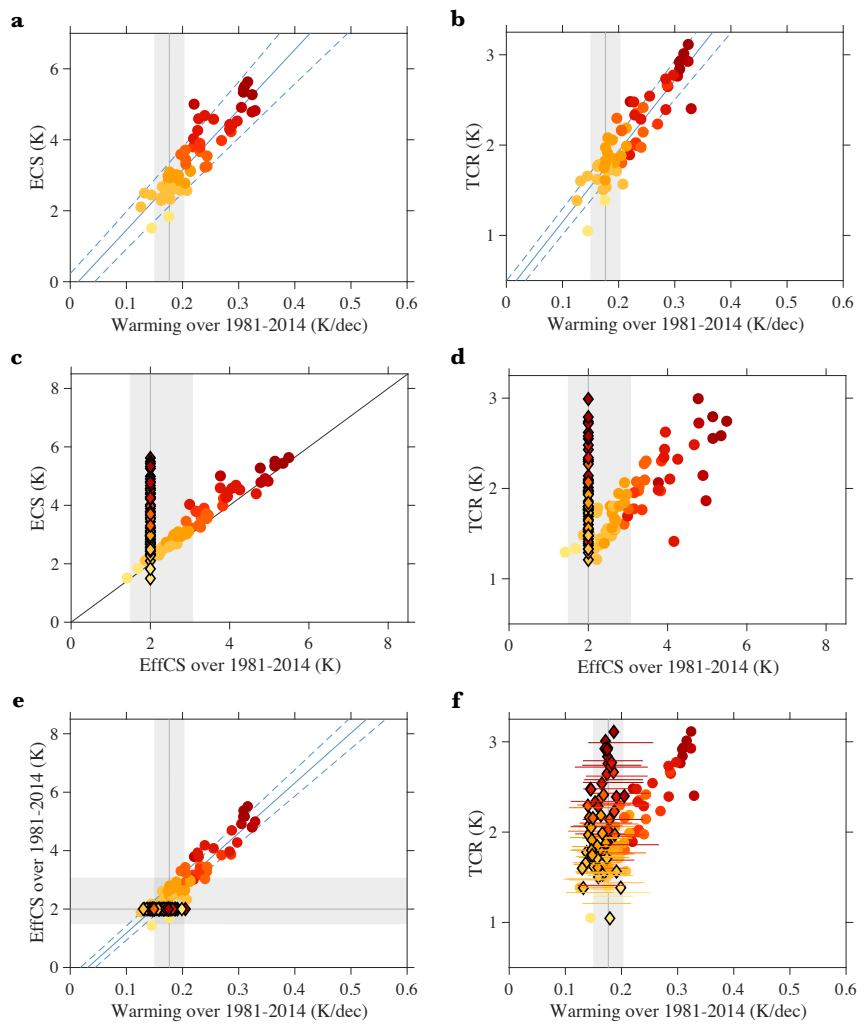


Fig. S5. Relationships between equilibrium climate sensitivity (ECS), transient climate response (TCR), effective climate sensitivity (EffCS), and the 1981-2014 warming rate in the two-layer energy balance model (EBM). **a**, ECS versus warming rate; colors correspond to values of ECS. **b**, TCR versus warming rate. **c**, ECS versus EffCS over 1981-2014; diamonds show an EffCS value corresponding to an observational estimate of 2°C. **d**, TCR versus EffCS over 1981-2014; diamonds show an EffCS value corresponding to an observational estimate of 2°C. **e**, EffCS over 1981-2014 versus warming rate; diamonds show warming rates simulated by the EBM when using an EffCS value corresponding to an observational estimate of 2°C over 1981-2014, which are in good agreement with the regression slope (blue line with dashed blue lines showing 5-95% ranges of fit parameters). **f**, Relationship between TCR and warming rate with circles showing uncorrected warming rates and diamonds showing corrected warming rates using observed values of EffCS as described in main text, with a median of 2°C and horizontal lines showing 5-95% confidence ranges showing 1.5-3.1°C. Gray shading shows observational estimates (5-95% range) of observed warming rate and EffCS as described in the main text.

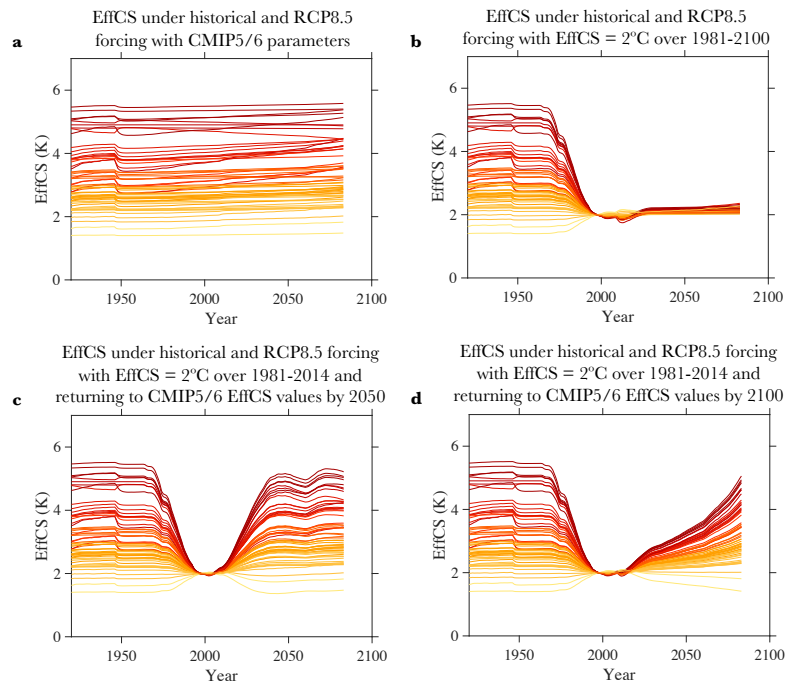


Fig. S6. Two-layer energy balance model (EBM) effective climate sensitivity (EffCS) under historical and RCP8.5 radiative forcing, either with CMIP5/6 model parameters or with prescribed changes in EffCS. a, EffCS using CMIP5/6 parameters; colors correspond to values of ECS. b, EffCS using CMIP5/6 parameters but with EffCS = 2°C over 1981-2100. c, EffCS using CMIP5/6 parameters but with EffCS = 2°C over 1981-2014 and EffCS returning to CMIP5/6 values by 2050. d, EffCS using CMIP5/6 parameters but with EffCS = 2°C over 1981-2014 and EffCS returning to CMIP5/6 values by 2100.

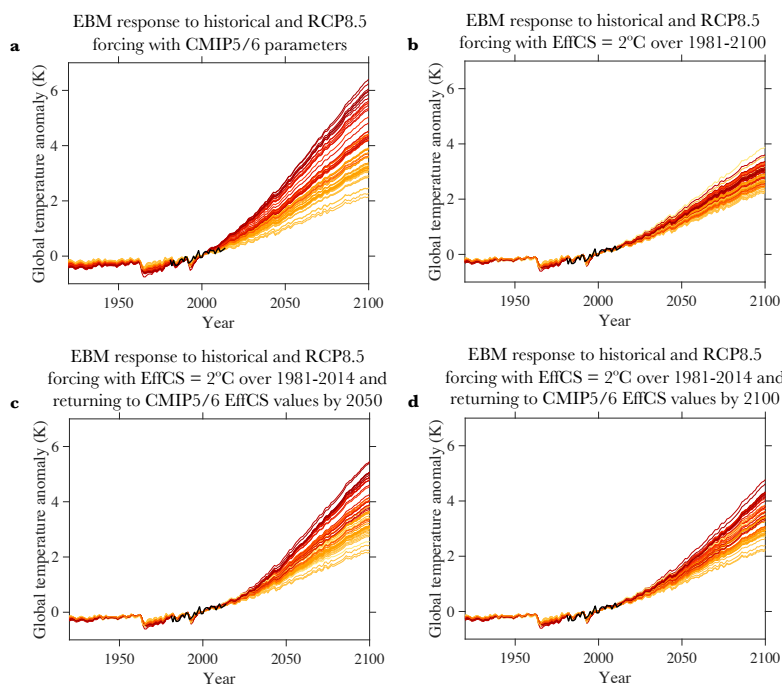


Fig. S7. Two-layer energy balance model (EBM) global surface temperature response to historical and RCP8.5 radiative forcing, either with CMIP5/6 model parameters or with prescribed changes in effective climate sensitivity (EffCS). a, Temperature anomaly using CMIP5/6 parameters; colors correspond to values of ECS. b, Temperature anomaly using CMIP5/6 parameters but with EffCS = 2°C over 1981-2100. c, Temperature anomaly using CMIP5/6 parameters but with EffCS = 2°C over 1981-2014 and EffCS returning to CMIP5/6 values by 2050. d, Temperature anomaly using CMIP5/6 parameters but with EffCS = 2°C over 1981-2014 and EffCS returning to CMIP5/6 values by 2100. Black lines show observed global surface temperature anomaly from HadCRUT5 over 1981-2014, and all anomalies are plotted with respect to the average over 1981-2014.